III.B.2 Lithium Sulfur Batteries

III.B.2.i. A New Lamination and doping Concepts for Enhanced Li – S Battery Performance (University of Pittsburgh)

Dr. Prashant N. Kumta, Principle Investigator
Organization: University of Pittsburgh
Address: 815C Benedum Hall ,3700 O'Hara Street
Pittsburgh, PA 15261
Phone: (412) 648-0223;
E-mail: pkumta@pitt.edu

Dr. Moni K. Datta, Co-PI
Organization: University of Pittsburgh
Address: 815C Benedum Hall ,3700 O'Hara Street
Pittsburgh, PA 15261
Phone: 412-648-0223 Fax: 412-624-3699
E-mail: mkd16@pitt.edu

Dr. Oleg I. Velikokhatnyi, Co-PI
Organization: University of Pittsburgh
Address: 815C Benedum Hall ,3700 O'Hara Street
Pittsburgh, PA 15261
Phone: 412-648-0223 Fax: 412-624-3699
E-mail: olv3@pitt.edu

Tien Duong, DOE Program Manager
Vehicle Technologies Office, U.S. Department of Energy
Phone: (202) 586-7836
E-mail: tien.duong@ee.doe.gov

Colleen Butcher, DOE Program Manager
US Department of Energy/NETL
Phone: 412-386-7341
E-mail: Colleen.Butcher@NETL.DOE.GOV

Start Date: October 2014 End Date: September 2017
Total Project Cost: $1,250,061 DOE share: $1,250,061 Non-DOE share: $0

Project Introduction

Lithium ion batteries (LIBs) clearly dominated the area of high-energy storage systems for the past decade with significant research and development activity focused on the development of cathode and anode materials to maximize the specific energy storage, stability, and cycle life of the batteries. However, with the increasing demand in the EV industry for low cost, low weight, and high-energy storage batteries to meet the *EV everywhere grand challenge*, the current focus of research has shifted towards the development of lithium sulfur batteries (LSB) owing to the high theoretical specific capacity exhibited by sulfur compared to other cathode materials currently available. Li–S battery shows a theoretical capacity of 1675 mAh/g corresponding

to the formation of Li_2S which makes sulfur a promising electrode to replace the layered transition metal oxides (~150 mAh/g) and $LiFePO_4$ (~170 mAh/g) hitherto deployed in present LIB systems. Moreover, the abundance of sulfur in the earth's crust makes it a more economical and highly attractive proposition compared to currently existing cathodes. Despite advantages of sulfur, the existing Li-S battery technology display poor cyclability, low coulombic efficiency (CE) and very low cycle life due to the following issues: 1. Polysulfide (PS) dissolution; 2. Sluggish kinetics of PS to Li_2S conversion; 3. High PS diffusivity in the electrolyte; 4. Insulating nature or poor conductivity of sulfur/Li_2S; 5. Volumetric expansion/contraction of sulfur; 6. Shuttling of PS along with Li^+. These issues result in loss of sulfur causing mechanical disintegration, surface passivation of both anode and cathode, thereby decreasing the specific capacity and columbic efficiency (CE). Present generation sulfur cathodes also show low specific storage capacity, very poor charging rates and low loading densities. Research is needed to overcome the issues impeding Li-S battery technology development.

Objectives

The objective of this project is to develop Lithium sulfur batteries capable of achieving the following performance requirements;

Energy Storage Performance Requirements		Electric Vehicle
Characteristics	Unit	
Specific Discharge Pulse Power	W/kg	700
Discharge Pulse Power Density	W/l	1,500
Specific Regen Pulse Power	W/kg	300
Recharge Rate	kW	1.4
Specific Energy	Wh/kg	350
Energy Density	Wh/l	750
Calendar Life	Year	15
Cycle Life	Cycles	1000
Operating Temperature Range	ºC	-30 to +52

Approach

The objectives outlined above will be accomplished by engineering sulfur cathode materials primarily by laminating the electrodes with lithium ion conductor (LIC) coatings to prevent polysulfide dissolution and doping of sulfur to improve the electronic and ionic conductivity. Major technological innovations will be undertaken to accomplish the following objectives in this effort:

Phase – 1 (Year 1): Synthesis, Characterization and Scale up of suitable LIC matrix materials and multilayer composite sulfur cathodes. This phase is completed.

Identify novel LIC coating materials and morphology for composite multilayer sulfur cathode architectures exhibiting: Specific capacity ≥1000 mAh/g (≥8 mAh/cm2), cyclability (~1000 cycles), loss per cycle ≤0.05% per cycle, Coulombic Efficiency (CE): ≥80%.

Phase – 2 (Year 2): Development of LIC coated sulfur nanoparticles, scale up of high capacity engineered LIC coated multilayer composite electrodes and doping strategies for improving the electronic conductivity of sulfur.

Optimize and scale up of the interface engineered (I.E.) multilayer composite LIC coated sulfur cathode architectures exhibiting: Specific capacity ≥1200 mAh/g (≥4 mAh/cm2), cyclability (~1000 cycles), loss per cycle: ≤0.01% per cycle, CE: ≥80%.

Synthesize and scale up of doped sulfur nanoparticles on gram scale and demonstrate improvement in performance, reflected as an increase in sulfur weight percentage and improvement in rate capability of cycling of the electrodes.

Phase-3 (Year 3): Advanced high energy density, high rate, highly cyclable cell development.

Tie together the three different trees of development i.e. coating development/sulfur particle development/CNT based exploration by identifying suitable configuration integrated electrode (I.E.) with maximum sulfur weight

percentage demonstrating high capacity ≥1400 mAh/g, cyclability (~1000 cycles), loss per cycle: ≤0.01% per cycle, CE: ≥80%.
Assemble 4 mAh high energy density Li-S pouch cells and performance testing.

Results

FY 2015 – (Q1-Q4)

The aim of Phase-1 of this project was essentially to identify various materials that can act as lithium ion conductors (LICs) while preventing polysulfide transport and accompanying sulfur loss. The end of Q-4 has a Go/No-go point which is based on the ability to demonstrate that the working hypothesis is valid (i.e. LICs improve Li-S battery cycle life). In order to achieve this target, 4 strategies were employed during Phase-1 of the project: (a) Use of inorganic LICs in the form of pellet coatings (Q1, Q2) (b) fabrication of flexible polymer-sulfur wires (Q2) (c) generation of gel polymer electrolyte (GPE) as an electrolyte medium (Q3) (d) use of complex framework materials (CFM) as trapping agents for sulfur species (Q4). The various strategies and progress achieved therein are described below:

High areal capacity inorganic LIC coated sulfur nanoparticulate electrodes

Research in the first quarter of Phase-1 involved identification of strategies to improve the characteristics of sulfur electrodes by pursuing a three-pronged approach:

a) Synthesis of nano-particulate sulfur in order to achieve higher capacities without significant increase in fade rate.
b) Use of solid state processing i.e. pellet pressing as an effective method to improve the capacity retention in lithium sulfur batteries in comparison to the conventional slurry casting procedure.
c) Coating of thin solid state lithium-ion conductive (LIC) layer for minimal contact of liquid electrolyte with sulfur preventing dissolution of the polysulfides formed during lithiation of sulfur, while at the same time not presenting problems observed with the use of purely solid state electrolytes.

Among the several approaches identified, the first was to synthesize sulfur nanoparticles (SNPs) size to increase the capacity approaching theoretical limits of sulfur (~1675 mAh/g-Sulfur). The synthesis procedure involved re-precipitation of sulfur dissolved in a basic media followed by acid-driven neutralization. Different concentrations of various molecular acids resulted in colloidal SNPs of various sizes determined by dynamic light scattering (DLS). The average particle size was observed to decrease with lower concentration of the dissolved sulfur solution and also with the decrease in the normality of the acid solution used for generating the colloidal SNPs. Among the various SNPs, particles of ~600 nm were found to have ideal electrochemical characteristics. Figure V-1a and Figure V-1b show the SEM images of the nano-sulfur and commercial sulfur, respectively. The difference in particle size can be distinctly observed by comparing the two images. The nano-sulfur particles formed by the chemical re-precipitation procedure exhibit agglomerated particle sizes of ~500 nm-2 μm as seen in the SEM micrograph in Figure V-1a. Commercially obtained sulfur particles used as precursors in the chemical re-precipitation reaction on the other hand, have a wide particle size distribution consisting of 20-150 micron particles as seen in Figure V-1b. The fine particles of nano-sulfur are expected to have exceptional exposure to the lithium conducting (LIC) layer/conductive additive resulting in high capacity. Similar to the case of nanoparticle amorphous silicon anodes studied for Li-ion batteries, reversible expansion and contraction would not result in particle fracture and accompanying capacity fade. Figure V-1c shows the morphology of the composite multilayer electrode assembled by the pellet pressing method. The pellet consists of a thin layer of lithium orthosilicate coating the mixture of sulfur and carbon. The uniformity of the coating and lack of macroscopic cracks are confirmed from the same. The inset images depict the disparate architecture existing within the orthosilicate layer and the sulfur-carbon layer. The orthosilicate layer consists of macroscopic particles fused together as a result of the mechanical pressing process. It can also be seen that the layer consists of macroscopic pores ideal for liquid electrolyte percolation. Short solid-state diffusion distances would result and the common issues typically experienced in solid electrolyte based lithium-sulfur batteries would thus be circumvented. The orthosilicate layer is a few microns

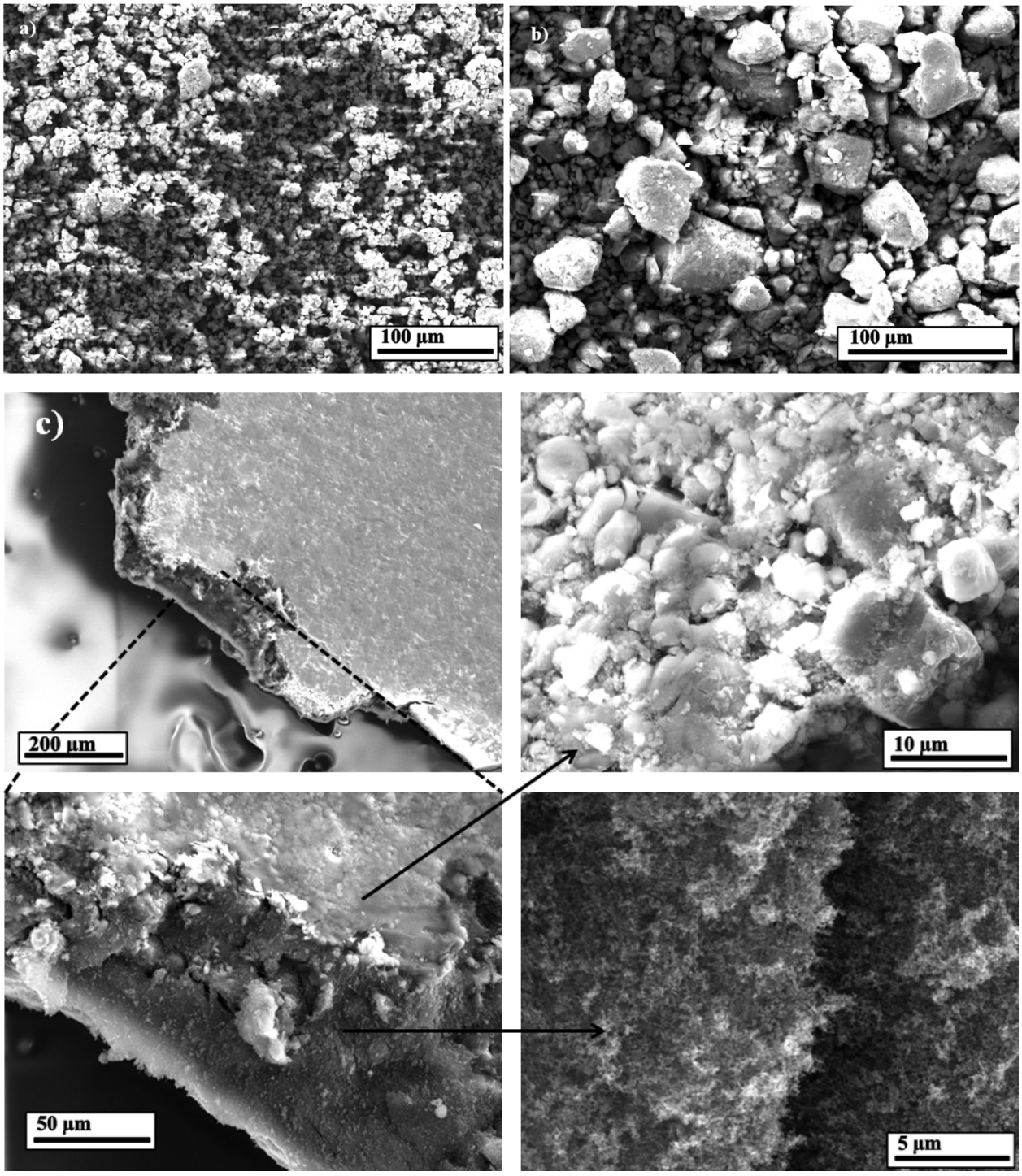

Figure V - 1: Scanning electron microscope images of a) Chemically derived nano sulfur; b) Commercially procured sulfur; c) Composite multilayer electrode architecture with a uniform coating of lithium orthosilicate on a sulfur-carbon mixture. The layer structure is clearly visible in the inset image. The top layer of orthosilicate is porous and consists of macroscopic particles fused as a result of the mechanical pressing. The soft sulfur-carbon inner layer consists of much finer particles of distinctly different morphology.

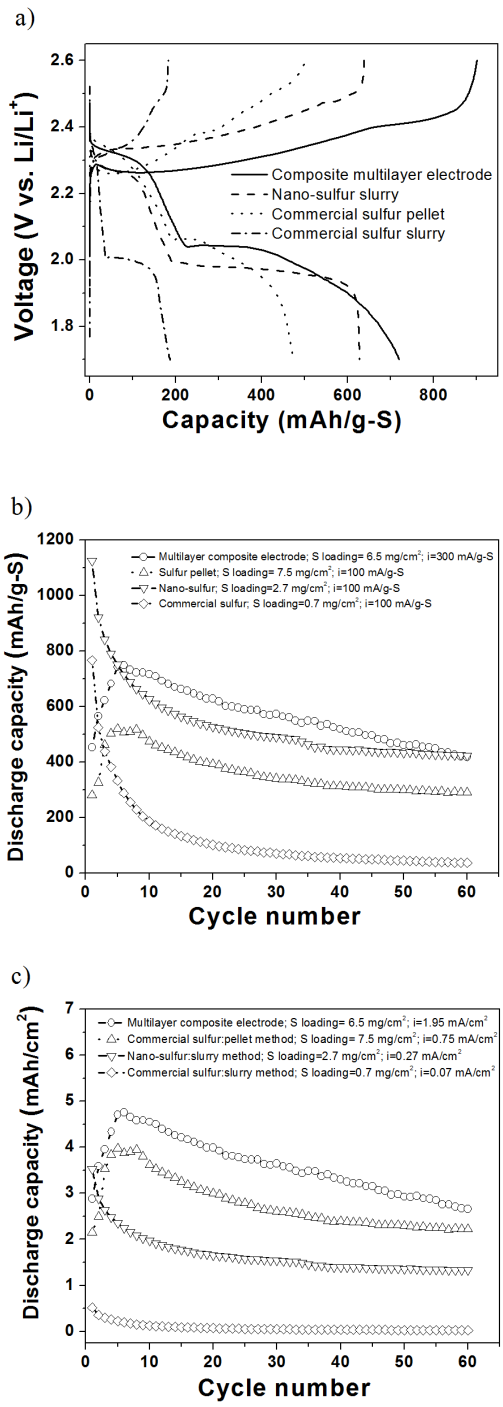

Figure V - 2: a) Charge-discharge profiles (sulfur basis gravimetric capacity) of the various electrode architectures; b) Comparison of cycling behavior of the commercial sulfur, nano-sulfur prepared by slurry method, pellet method and the multilayer composite electrode; c) Comparison of cycling

thick ensuring that sulfur particles are not directly exposed to the liquid electrolyte thus serving to protect and prevent any dissolution of the polysulfides formed. The channel structure existing in the electrode would thus

ensure minimal percolation of liquid electrolyte to sulfur particles. In addition to the protection offered by the orthosilicate layer, the pressing procedure ensures the formation of an elegant carbon coating on the sulfur particles. The carbon networks thus act both as electron conducting and lithium ion conducting (LIC) channels. Solid-state lithium ion diffusion through carbon is not hindered and should not pose as a barrier to the ensuing intercalation and de-intercalation processes. Evaluation of electrochemical performance of the various sulfur materials as cathodes was thus performed for the electrodes generated following two methods. Electrodes of sulfur-carbon (1:1) were prepared by either tape casting from the organic solvent based slurries or mechanically pressed pellets. Figure V - 2a shows the 10th cycle charge-discharge profiles of the various sulfur-carbon materials. Characteristic plateaus corresponding to polysulfide formation and subsequent conversion to dilithium disulfide (Li_2S_2) and dilithium sulfide (Li_2S) are observed in all the materials. The composite multilayer electrode can be seen to exhibit however, the highest gravimetric capacity of the various materials after 10 cycles as a result of the high capacity yielded by the nano-sulfur (as shown in Figure V - 2b also). The nano-sulfur slurry electrode also displays a high capacity as compared to the commercial sulfur pellet and the slurry made from commercially obtained sulfur powder. The cycling stability of the various materials is plotted in Figure V - 2b and Figure V - 2c (specific gravimetric and areal capacity, respectively). Among the slurry cast electrodes, it can be seen that the nano-sulfur demonstrates the higher capacities and better fade characteristics in comparison to the commercially obtained sulfur. The improvement in capacity can be attributed to the change in particle size seen in **Figure V - 1**a and **Figure V - 1**b. The higher surface area of the 0.3-2 μm particles (as confirmed by DLS) results in enhanced reactivity and thus better capacity. The improvement in cycling performance observed therein could be attributed to reduced particle stresses in smaller particles resulting in much reduced fracture and delamination. In addition, the fine particle size would ensure good contact with the conductive additive preventing the particles from becoming inactive over time as a result of the fracture. The crystalline nature of the fine nanoparticles would at the same

time, ensure that the particles would not be completely insulating. The slurry cast nano-sulfur electrode thus has a high initial capacity of ~1125 mAh/g-S and a fade rate of 0.86%/cycle as seen in Figure V - 2b. This superior performance indicates that sulfur behaves similar to silicon with respect to charge storage capability and cycling stability, in that the reduction in particle size aids both those characteristics. The nano-sulfur slurry cast electrode has a high initial areal capacity of 3.5 mAh/cm^2, stabilizing at ~1.4 mAh/cm^2, upon further cycling (Figure V - 2c).

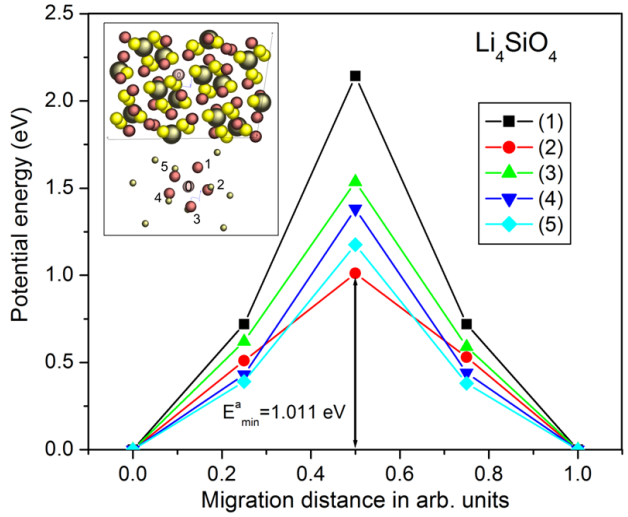

Figure V - 4: Activation barriers for different migration paths of Li-ions in Li_4SiO_4. Inset: pink 0 - Li-ion site; red (1)-(5) – Li vacancy sites for different migration pathways.

The improvement in charge storage as a result of utilizing the pellet-pressing procedure, especially the composite multilayer electrode architecture is both seen in Figure V - 2b. The use of the pellet pressing procedure yields thicker electrodes, while at the same time allowing for better capacity retention. This results in the significantly higher areal capacities seen in Figure V - 2c. The thick electrodes made from commercially obtained sulfur have an initial areal capacity of ~4 mAh/cm^2 while the composite multilayer electrode has an areal capacity of ~4.75 mAh/cm^2. These are values corresponding to the 5th cycle since these thick electrodes suffer from poor wetting in the initial cycles as would be expected. With further optimization, we believe we could improve the capacity and cyclability of the electrodes by ensuring that polysulfides would not contribute to loss of electrical contact and would thus get completely converted to Li_2S. Even so, the capacity at the 5th cycle is much higher than the current EERE-OVT (Office of Energy Efficiency & Renewable Energy-Office of Vehicle Technologies) target for areal capacity of electrodes of 4 mAh/cm^2. It should be also noted that the areal capacities and sulfur loadings on the electrode exceed those previously reported though further optimization is ongoing to improve the overall sulfur weight percentage (to reduce overall electrode thickness). Both electrodes exhibit superior cycling stability though validating the hypothesis that the inorganic LIC materials aid in preventing polysulfuide dissolution driven lithium-sulfur battery capacity loss hitherto seen.

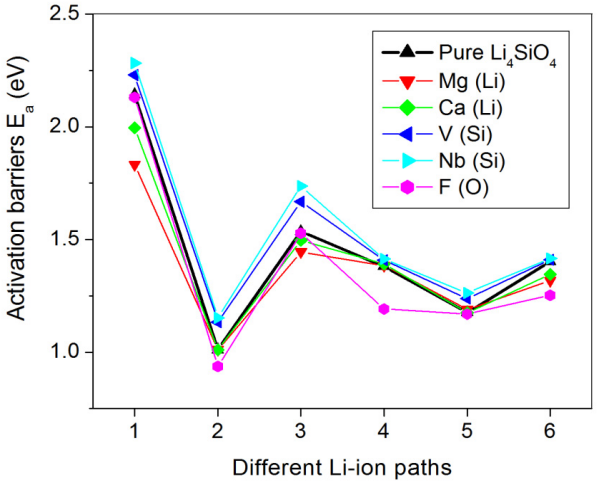

Figure V - 3: Activation barriers Ea for different migration paths of Li-ions in pure and doped Li_4SiO_4.

First principles studies into identification of high ionic conductivity LIC coating materials

Improvement in LIC ionic conductivity and polysulfide filtration capability is to be acheived by first principles driven design and experimental development of suitable LIC materials with the aim of further improving cycing capability. Using the nudged elastic band method implemented in VASP (Vienna ab-initio simulation package), various Li-ion migration pathways have been considered and corresponding activation barriers Ea have been calculated. Corresponding results in Figure V - 4 indicate that the pathway (0-2) requires the lowest activation energy (~ 1 eV) for the Li-

ion migration from the central position (0) to the Li-vacancy (2). All other pathways demonstrate higher activation barriers (up to 2.2 eV). Introduction of aliovalent dopants could create Li-ion vacancies as well as decrease the activation barriers for the ionic migration, thus improving the overall ionic mobility. The ionic conductivity of doped Li_4SiO_4 with Mg, Ca, V, Nb, and F has been studied from first principles. Corresponding results shown in Figure V - 3 indicate that Mg^{2+} and Ca^{2+} replacing Li^+-ion as well as F^- replacing O^{2-} ions help decrease the activation barriers for all corresponding Li-ion pathways in comparison to pure Li_4SiO_4. On the other hand, V and Nb substituting Si-ions slightly increase the E_a due to the larger ionic radii of V^{5+} and Nb^{5+} vs. Si^{4+}. However, the overall Li-ion conductivity is expected to be improved due to formation of Li^+ vacancies and thus, facilitating Li-ion hopping through the crystal lattice. In terms of structural and chemical stability, calculated cohesive energies of the pure and doped orthosilicates indicate that V and Nb slightly decrease the stability, while Mg, Ca and F virtually rener the stability invariant. Thus, the present theoretical study helped in identifying Mg, Ca, and F as prospective doping elements facilitating improvement in the Li-ion conductivity without sacrificing the overall structural and chemical stability of the LIC orthosilicate. An experimental validation of this conclusion will be conducted in the closest future.

Flexible polymer-sulfur wires

Following earlier studies demonstrating significant capacity and stability improvement in sulfur cathodes obtained by using a thin layer of lithium ion conductor (LIC) on sulfur nanoparticles, work in the second quarter involved identification of strategies to futher improve the stability by tailoring the sulfur morphology. Towards this end, flexible sulfur wires (Flex-SWs) were generated using a simple polymer-handling method reported in Q2. The synthesis allows for a polymer-sulfur wire morphology (Figure V - 5) to be obtained with the polymer acting as a structural template as well as improveing the cycling characteristics by facilitating polysulfide retention. Figure V - 6a and Figure V - 6b depict the scanning electron micrograph and corresponding sulfur map of the unique sulfur fiber (Flex-SW) morphology obtained for the first time rendering Flex-SW very amenable for use in compliant, flexible batteries. Figure V - 5 displays the yarn-like quality of the Flex-SWs opening the door for a multitude of unique applications. It can be seen from Figure V - 6b that sulfur is uniformly distributed over the length of the yarn with no obvious segregation. The unique synthesis procedure yields wires which are in-effect encapsulated in a polymer matrix thus directly addressing the primary problem of polysulfide dissolution typically solved by the ubiquitous

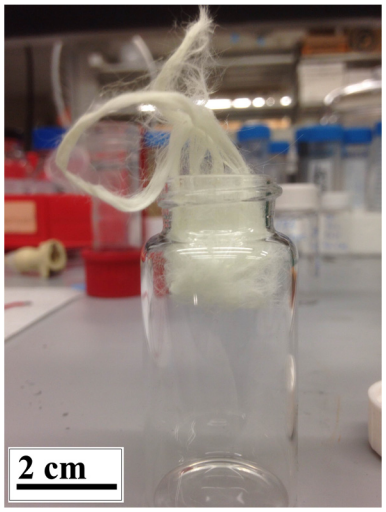

Figure V - 5: Image showing the yarn-like nature of the Flex – sulfur wires (Flex-SWs).

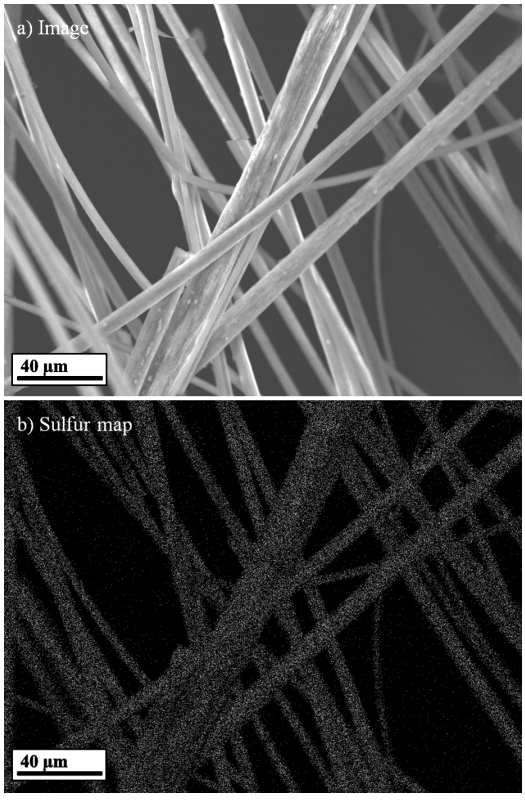

Figure V - 6: (a) SEM image (b) EDAX map of the flexible sulfur-polymer morphology shown in Figure V - 5.

chemically induced steric hindrance methods. Figure V - 7a shows the cycling response of the various sulfur electrodes including commercial sulfur cast (C-Sulfur:slurry) and pellet-pressed (C-Sulfur pellet); nano-sulfur pellet-pressed with an LIC layer (nano-Sulfur-LIC pellet); Flex-SWs with LIC (Flex-SW pellet-LIC) and void LIC (Flex-SW pellet) layers. The Flex-SW pellet demonstrates superior stability and minimal capacity fade over ~135 cycles (see Figure V - 7b). The Flex-SW pellet demonstrates an initial capacity of ~700 mAh/g which stabilizes to ~450-500 mAh/g over the first 5 cycles. Studies are on-going to understand this stabilization behavior, a typical feature of Flex-SW materials. This 1st cycle irreversible loss behavior however is circumvented by use of a thin LIC coating on Flex-SW as seen in Figure V - 7a wherein the FSW-LIC pellet maintains a stable capacity of ~650 mAh/g over 60 cycles (fade rate~0.003%/cycle). Further analysis and optimization is ongoing to improve the capacity and stability of the flexibl e sulfur- polymer wires. Stable areal capacity of the Flex-SW-pellet materials is ~2.5 mAh/cm^2 and optimization of sulfur weight percentage is needed to improve this number to achieve the targeted 4 mAh/cm^2.

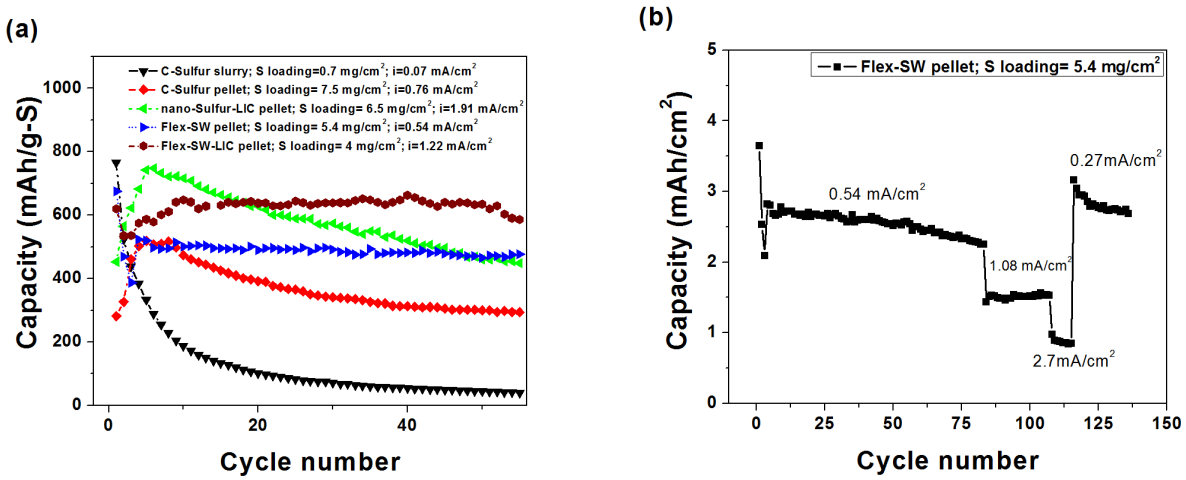

Figure V - 7: (a) Cycling behavior of various sulfur materials (b) Extended cycling and rate dependence of capacity in Flex-sulfur wires seen in Figure V-6.

Polymeric LIC materials (Gel-polymer electrolyes-GPEs)

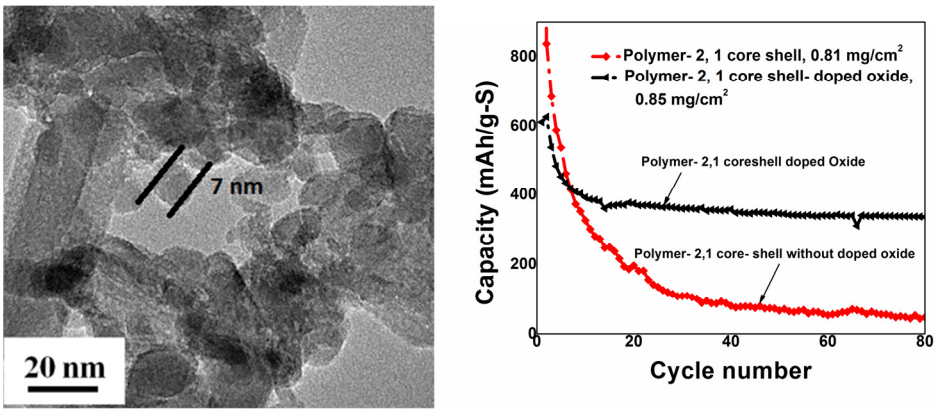

Figure V - 8: (a) Transmission electron microscope (TEM) (left Fig.) of oxide nanoparticles used as fillers in the GPE materials (b) Effect of oxide filler material on cycling behavior in polymer LIC materials (right Fig.).

In addition to inorganic LIC materials, polymer LIC (gel-polymer materials (GPE) containing lithium-ion conductor) materials were explored as a part of continuing studies into the same. These polymeric LIC materials were used in place of conventional polymeric separator materials. Figure V - 9 depicts the improvement in cycling stability of creating composite polymeric core-shell and layer-by-layer composite materials. In order to tackle fade associated with the gel-polymer electrolyte materials, nanoparticulate oxide materials were used as fillers in the GPE matrix. Figure V - 8a shows the TEM images of the oxide nanoparticles used therein and Figure V - 8b depicts the improvement in cycling behavior occurring as a result of the same.

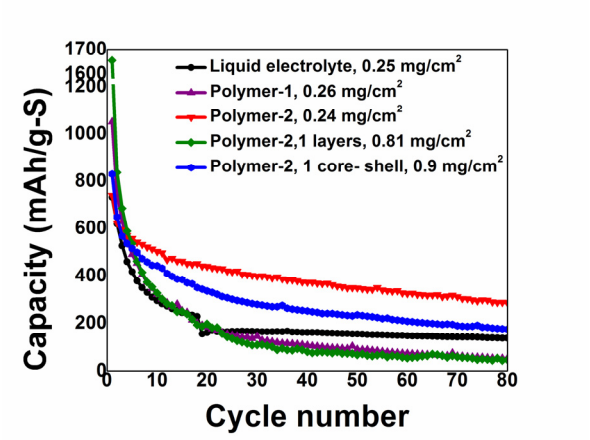

Figure V - 9: Comparison of cycling behavior of various polymeric LIC electrolyte materials.

Stability as a result of using doped oxide nanoparticles as filler materials in the polymer material results in a stable capacity of ~400 mAh/g seen upto 80 cycles. The polymer electrolyte materials with oxide tethering sites act as both polysulfide filters as well as restainment media ensuring improvement in cycling stability. Optimization work is ongoing involving the gel-polymer LIC electrolyte materials and will be reported in following reports.

Complex framework materials (CFM)

Research on Li – S batteries is mainly focused on three main aspects:(i) Improving the conductivity of Sulfur by using conductive coatings or composites and hence increasing the active material utilization, (ii) Modifying the liquid electrolyte – separator system using a gel – polymer or composite – polymer electrolyte to prevent polysulfide dissolution and (iii) Confining sulfur into porous matrices and hence preventing polysulfide dissolution. Porous materials with pore size comparable to or less than the size of polysulfide species need to be devised in order to completely overcome the problem of polysulfide dissolution. Hence, the use of complex framework materials (CFM) as trapping agents for sulfur species has been explored. The CFM materials containing nanopores are ideal for entrapping the soluble polysulfide species formed during lithiation of sulfur. Figure V - 10 depicts the morphology of certain nanoporous CFMs acting as sulfur – hosts. There is a significant improvement in initial capacity and cycling stability as a result of

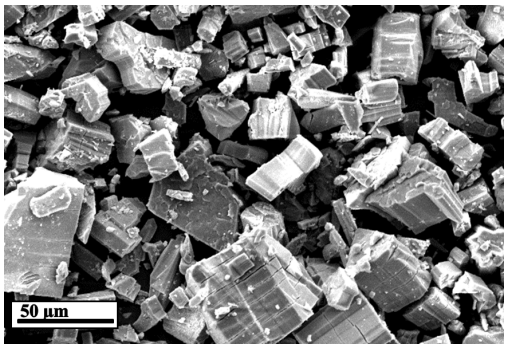

Figure V - 10: Morphology of sulfur-containing nanoporous CFMs.

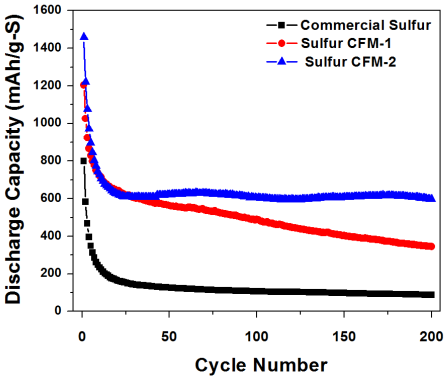

Figure V - 11: Improvement in cycling stability of sulfur cathodes by use of CFM materials.

Table V - 1: Cycling characteristics of various sulfur battery systems synthesized and evaluated in this work.

Material	Initial discharge capacity (mAh/g-S)	Initial capacity fade¥ (% capacity)	Fade rate* (% capacity/cycle)
C-Sulfur:slurry	766.3	56.53	1.76
C-Sulfur pellet	519.3†	N/A	0.87
nano-Sulfur-LIC pellet	748.2†	N/A	0.79
Flex-SW pellet	675.4	23.09	0.17
Flex-SW pellet-LIC	620.3	5.37	0.003
Polymer 2,1 core-shell-doped oxide	776.26	36.75	0.4
Sulfur CFM-2	1460.4^	54.79	0.01

¥Fade rate calculated on the basis of 1st cycle capacity and 5th cycle capacity.*Fade rate calculated on the basis of 5th cycle capacity and 55th cycle capacity. †Capacity reported at 5th cycle since there was an increase in capacity from 1st cycle due to gradual wetting of the electrode.^Stabilizes at 20th cycle and fade calculated upto 200th cycle.

the use of sulfur-containing CFMs as Li-S battery cathodes and stable cycling has been demonstrated for up to 200 (Figure V - 11) cycles thus-far (further cycling is ongoing). The CFM electrodes exhibit a very low fade rate of ~0.01%/cycle following initial phase change.

FY 2016-(Q1-Q4)

The aim of Phase-2 studies is to synthesize novel doped LIC materials with high lithium ion conductivity identified in Phase 1, to develop effective coating strategies of these materials and to generate hetero structured composites of sulfur with carbon materials. Towards this end, the following strategies were employed during Phase-2 of the project: (a) Improving ionic conductivity of lithium ion conductors using first-principles driven doping approaches (b) Composite polymer electrolytes demonstrating no capacity loss in commercial sulfur electrodes (c) Sulfur infiltrated framework (SFM) materials with chemical trapping of sulfur (d) Altering the electronic structure of sulfur with size matched dopants. The results of these studies are listed below:

Improving ionic conductivity of lithium ion conductors using first-principles driven doping approaches

In FY14, it was demonstrated using density functional theory (DFT) studies that an improvement in ionic conductivity can be achieved upon the introduction of vacancies in the lattice of Li ion conductor Li_4SiO_4. Li_4SiO_4 is a very wide band gap insulator with strong Si-O hybridization, covalent Si-O bonds and ionic Li-O, large channels for Li-conduction with Li^+ ionic conductivity (~ 10^{-12} S/cm). The effect of doping (dopants-D_1 and D_2) on Li sites and F doping on O sites of Li_4SiO_4 on its ionic conductivity was investigated using first principles calculations in Phase-1. Nudged elastic band method has been used for determining the potential energies and activation barriers E_a for various Li-ion migration pathways in pure and doped Li_4SiO_4. These calculations suggest a decrease in the activation barrier (**Figure V - 12**) for Li^+ ion conductivity because of doping. The unit cell of Li_4SiO_4 contains two SiO_4^{-4} tetrahedra linked by 8 lithium ions, which are distributed over 18 possible sites. At room temperature, an improvement in ionic conductivity of 3 to 4 orders in magnitude could be obtained by forming simple solid solutions.

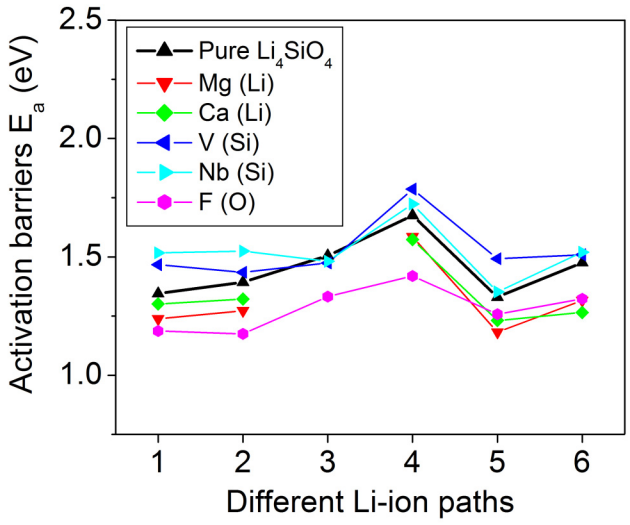

Figure V - 12: Activation barriers E_a (eV) for different migration paths of Li-ions in pure and doped Li_4SiO_4.

To validate the theoretical predictions, cation and anion doping of Li_4SiO_4 was performed to obtain final materials of the chemical formula shown by i and ii.

i. $(Li_y[\ ]_xY_x)_4SiO_4$, where Y – D_1, D_2, [ ] – vacancy, x – 0.025 to 0.15
ii. $Li_4Si(O_y[\ ]_xZ)_4$, where Z – D_3, [ ] – vacancy, x – 0.025 to 0.15

Solid state high temperature processing route from suitable precursors was employed to generate doped nanoparticles of LIC. Different precursor ratios were used to tailor the atomic % of lithium vacancies in the LIC and tested for ionic conductivity. Lithium orthosilicate was doped with six different concentrations (2.5 at. %-15 at. %) of each dopant using a high temperature solid state diffusion technique. The X-ray diffraction (XRD) patterns of the various compositions of doped lithium orthosilicate indicate that a maximum of 7.5% lithium sites was successfully doped with the two different cations (D_1 and D_2). Further increase in the dopant concentration results in formation of secondary phases. Similarly, up to 7.5% oxygen sites were replaced with dopant D_3 maintaining phase purity, with secondary phases appearing upon excessive D_3 doping. **Figure V-13(a-c)** show the results of electrochemical impedance spectroscopy (EIS) analysis of the doped lithium orthosilicate materials and **Figure V-13d** depicts the ionic conductivity dependence on dopant concentration in the various doped materials. Creation of vacancies in the LIC crystal structure by doping with D_1 (~7.5 at. %) resulted in an increase in ionic conductivity from 1.179×10^{-12} S cm^{-1} to 2.870×10^{-8} S cm^{-1} as seen in **Figure V-13d**. Doping with D_2 (7.5at. %) and D_3 (10 at. %) results in a 3-order improvement in the ionic conductivity occurring close to the highest doped concentration (**Table V 2**). A comprehensive study utilizing sputter deposition technique to form uniform ultrathin coatings of LIC onto sulfur heterostructures is currently ongoing. These doped materials are currently being tested as LIC coatings in nano-sulfur based materials.

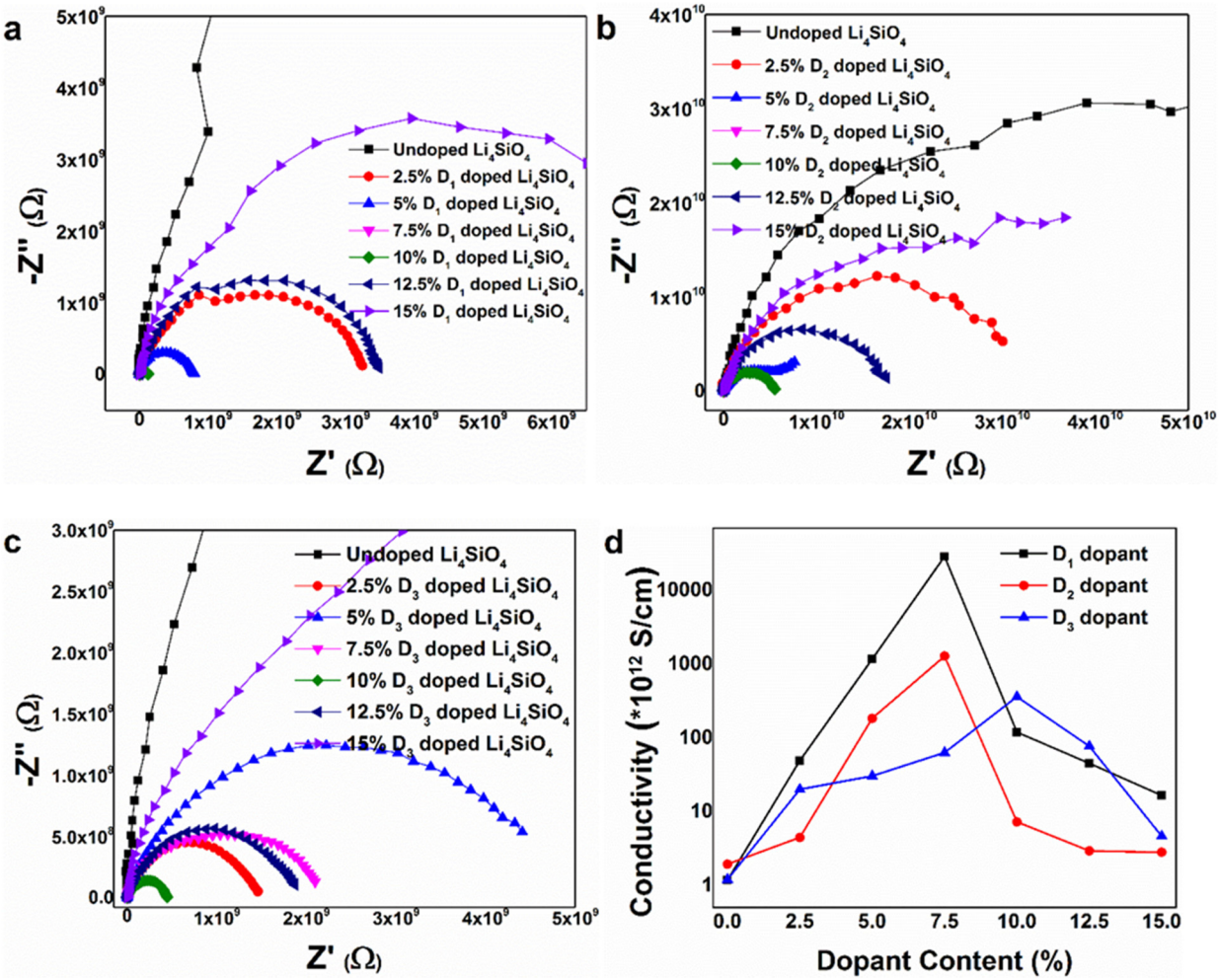

Figure V - 13: a) AC impedance based conductivity analysis of D_1 doped Li_4SiO_4; b) AC impedance based conductivity analysis of D_2 doped Li_4SiO_4; c) AC impedance based conductivity analysis of D_3 doped Li_4SiO_4 and d) Effect of doping D_1, D_2 and D_3 on the conductivity of Li_4SiO_4.

Table V - 2: Lithium ionic conductivities of Li_4SiO_4 upon doping with three different dopants D_1, D_2 and D_3.

	D_1 doped ($\times 10^{12}$ S/cm)	D_2 doped ($\times 10^{12}$ S/cm)	D_3 doped ($\times 10^{12}$ S/cm)
Li_4SiO_4 – undoped	1.16	1.29	1.19
2.5% doped	49.13	4.44	20.04
5% doped	1169.55	183.51	30.41
7.5% doped	28706.06	1277.59	63.13
10% doped	119.26	7.22	359.62

12.5% doped	45.08	2.93	76.95
15% doped	16.53	2.80	4.66

Composite polymer electrolytes (CPE) demonstrating no capacity loss in commercial sulfur electrodes

Work in Phase-1 of this project involved generation on lithium ion conducting polymeric membranes (LICMs) i.e. gel polymer electrolytes (GPEs) for use as separators in lithium-sulfur batteries. These polymeric LICM materials were used in place of conventional polymeric separator materials and it is expected that they will exhibit superior mechanical properties, flame-resistance and flexibility. To tackle capacity fade associated with the conventional gel-polymer electrolyte materials without fillers, nanoparticulate solid state materials were used as fillers in the GPE matrix. Stability improvement because of using doped solid-state nanoparticles as filler materials in the polymer material resulted in a stable capacity of ~400 mAh/g seen up to 80 cycles. The LICMs with solid state systems acting as tethering sites serve as filters to restrain the polysulfide ensuring improvement in cycling stability. Continuing optimization work into the same undertaken as a part of Phase-2 included engineering of the nature of the LICM materials with regards to polymer composition, filler material composition, particle size and porosity.

As a subtask of Q2, a free standing solid state system incorporated polymer membrane (SSPM) was used as a sieve to restrain the polysulfides from reaching the anode. The SSPM was used in addition to commercial separator to test with commercial sulfur cathode. Incorporation of the SSPM improved the specific capacity of commercial sulfur to ~550 mAh/g for over 100 cycles. This improvement in specific capacity arises from the binding of the polysulfide species onto the solid state functional moieties. Q4 of Phase – 2 involved the development of composite polymer electrolytes (CPE) with solid-state fillers using simple wet-chemical techniques that demonstrated high capacity and prevention of polysulfide dissolution. The CPE demonstrated an electrolyte uptake of ~200 wt% (**Figure V-14a**) with room temperature ionic conductivities (**Table V - 2)** similar to organic liquid electrolytes. In addition, it can be seen in **Figure V-14b** and **Figure V-14c** that the CPE materials possess significantly better mechanical properties (**Table V – 3**) and flame-resistance as compared to commercial separators making them ideal candidates for use in a lithium anode based system on account of improved safety. Testing of these CPEs with commercial sulfur cathodes showed an initial capacity of ~894 mAh/g which remained very stable demonstrating capacity of ~809 mAh/g after 50 cycles (**Figure V-14d**). Commercial sulfur electrodes normally undergo capacity loss to <100 mAh/g after 10 cycles. Thus, the CPE material demonstrates significant advancement in sulfur electrolytes. The cycling stability of the cathodes tested with CPE is likely due to the physical properties and optimized electrolyte content of these separator – electrolytes.

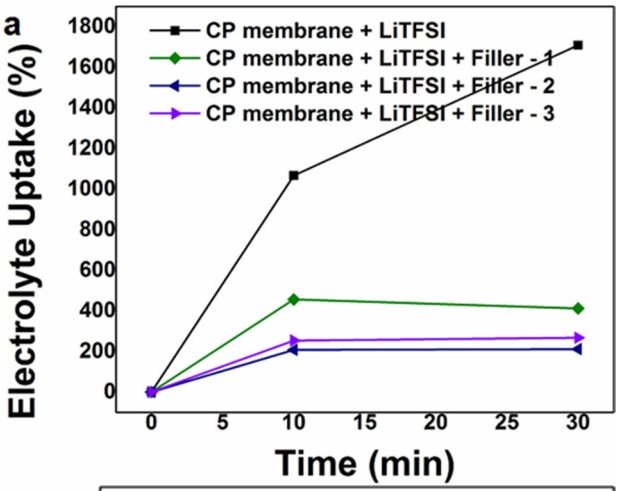
a
Electrolyte Uptake (%)
1800
1600
1400
1200
1000
800
600
400
200
0
CP membrane + LiTFSI
CP membrane + LiTFSI + Filler - 1
CP membrane + LiTFSI + Filler - 2
CP membrane + LiTFSI + Filler - 3
0
5
10
15
20
25
30
Time (min)

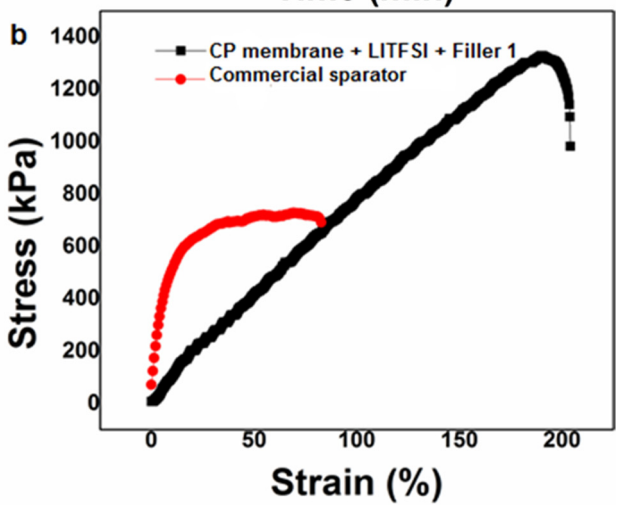
b
Stress (kPa)
1400
1200
1000
800
600
400
200
0
CP membrane + LITFSI + Filler 1
Commercial sparator
0
50
100
150
200
Strain (%)

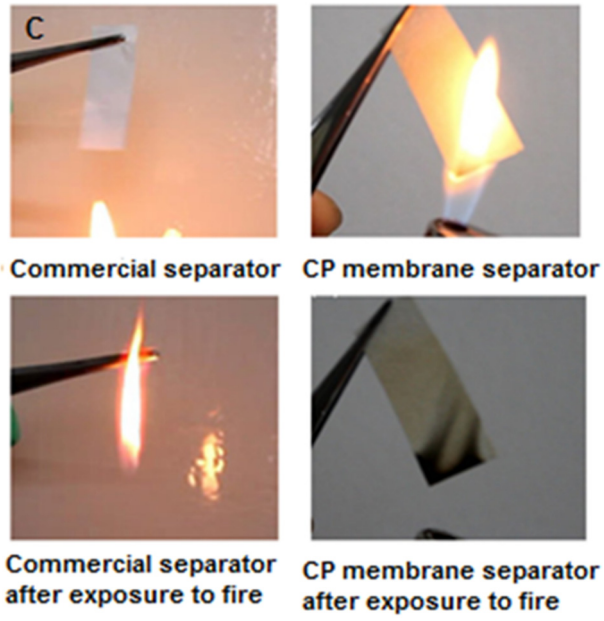
C
Commercial separator
CP membrane separator
Commercial separator after exposure to fire
CP membrane separator after exposure to fire

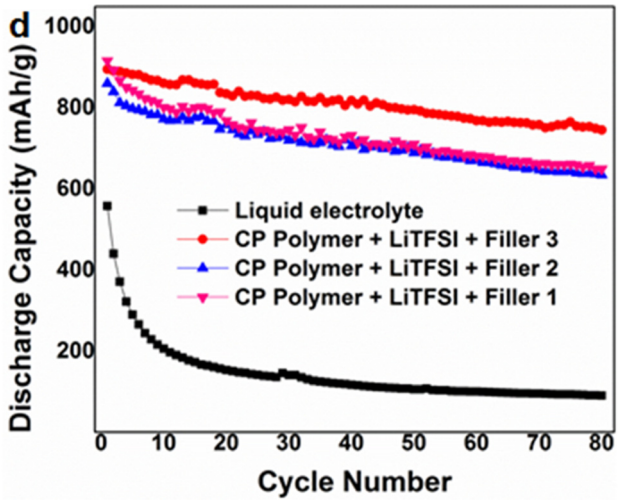

Figure V - 14: (a) Electrolyte uptake of CPE membranes

(b) Mechanical properties of the CPE membrane

(c) Flame-test depicting the superior safety of the CPE materials

(d) Cycling behavior of CPE membranes.

Table V - 3: Lithium ion conductivities of commercial separator compared with composite polymer membranes with three different fillers.

Sample Composition	Conductivity (S/cm)
Commercial separator with liquid electrolyte	$1.283*10^{-3}$
CP membrane + LITFSI + Filler 1	$1.881*10^{-3}$
CP membrane + LITFSI + Filler 2	$3.009*10^{-3}$
CP membrane + LITFSI + Filler 3	$9.4749*10^{-3}$

Table V - 4: Comparison of the mechanical properties of CP membrane and commercial separator.

Mechanical properties	CP membrane separator	Commercial separator
Tensile strength (kPa)	1114.8	636.1
Elongation break (%)	107.9	95.2
Young's modulus (GPa)	11.8	10.6

Altering the electronic structure of sulfur with size matched dopants

Another essential challenge this work aims to undertake is to increase the overall electrode capacity in sulfur cathodes by increasing the inherent electronic conductivity of sulfur. Towards this end, first principles studies were performed in Phase-1 of the study and suitable doping elements were identified to modify the electronic properties of sulfur resulting in its transformation from an insulator material to a semi-conductor/metallic conductor. Q3 of Phase – 2 also involved successfully doping commercially obtained sulfur (S_8) with similar sized dopants (**Figure V-15** shows the XRD patterns of doped S) to alter the electronic structure and enhance the electronic conductivity of S. A comprehensive study of the effect of doping of sulfur on rate capability is ongoing.

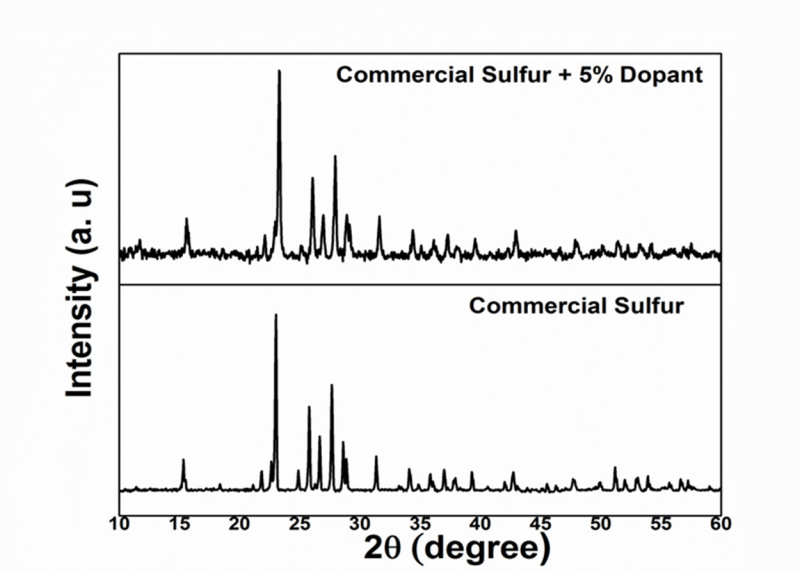

Figure V -15: XRD pattern of synthesized doped sulfur material showing phase-purity and peak shift.

Sulfur infiltrated Framework (SFM) materials with chemical trapping of sulfur

A final portion of the study in Phase-2 involved the use of framework materials to host sulfur and entrap polysulfides during cycling, and ensure capacity retention. The strategy with such host-based framework is two-pronged as follows: (a) the host acts as a conductive matrix; and (b) polysulfide species formed during lithiation are trapped inside the host matrix. Work in Phase-1 had identified complex framework materials (CFM) with sulfur infiltrated into the nanopores demonstrating very stable cycling with fade rates <0.01% loss per cycle after a short initial capacity fade. Despite improvements in stability, these structures exhibit an initial capacity loss, the origin of which was explored using X-ray photoelectron spectroscopy studies. Two variants of sulfur infiltrated CFMs, CFM-1 and CFM-2 were synthesized at room temperature and infiltrated with sulfur. The CFMs were used as cathodes for Li – S batteries. CFM-1 shows a very high initial capacity of 1476 mAh g^{-1}, which is the highest capacity value reported in the literature to date[1-3], stabilizing at 609 mAh g^{-1} over 200 cycles. The almost negligible fade rate (0.0014% loss $cycle^{-1}$) and complete prevention of polysulfide dissolution makes these cathode systems most promising candidates for Li-S batteries. However, there is an initial loss in capacity observed and to address this initial capacity loss observed in this system, the mechanism of lithiation and any other associated side reaction (e.g. SEI formation) involved in the electrochemical lithiation process needs to be understood. To rationally design sulfur hosts using complex framework materials (CFM), a basic understanding of the mechanisms involved in trapping polysulfide into the host materials needs to be established. This mechanism would further explain the origin of irreversible capacity loss during the initial cycles. The work uses

XPS analysis as a technique to understand the mechanism involved in masking polysulfide dissolution by directly binding the sulfide species onto the CFMs. The proposed concept of using chemical bonding has been reported elsewhere although complete prevention of polysulfide dissolution and retention has not been reported in the open literature to date[4]. The XPS technique was accordingly used to study polysulfide dissolution and to understand S – CFM bonding providing insight into prevention of the polysulfide dissolution in the current work. The mechanistic overview provided by this report could in our opinion lay the foundations and further identify possible pathways for implementing future design strategies to enhance the capacity and directly aim to resolve polysulfide dissolution problems in the initial cycles plaguing the Li-S battery cathodes.

Table V – 5 represents the BET specific surface area and average pore sizes of both the CFM materials. Both materials exhibit a very high surface area of ~ 526 $m^2 g^{-1}$, and ~684.25 $m^2 g^{-1}$, respectively with an average pore size of ~2. 47 nm. The CFMs were found to have high pore volume of ~0.324 $cm^3 g^{-1}$ and ~0.422 $cm^3 g^{-1}$. To prove the nanoporous nature of CFMs and the binding of sulfur to CFM, TEM analysis was employed **(Figure V-16)**. It is noteworthy that these surface areas are greater than those of most carbonaceous host materials that have reportedly been used as sulfur hosts in Li – S batteries[5-8]. The large pore volume of the CFM materials is expected to facilitate in ensuring larger amounts of sulfur encapsulation and thus high sulfur loading in the electrodes. Another unique advantage yielded using CFM materials to encapsulate sulfur is the small average pore diameter of the CFMs (2.46 nm) that aids in minimizing polysulfide dissolution by offering a better mode for trapping and confining the polysulfide species.

The TEM images of CFM-1 at a lower magnification (**Figure V-16a**) shows the highly porous nature of the CFM. Phase contrast image of S infiltrated CFM-1 (**Figure V-16b**) clearly shows ~5nm islands of sulfur inside the parent CFM structure indicating sulfur infiltration into the CFM. **Figure V-16c** demonstrates the local-ordering in the CFM structure. The nature of sulfur inside the CFM structure can be seen in **Figure V-16 d** wherein clear lattice fringes corresponding to sulfur infiltrated within the CFM structure are observed. Two different values of d – spacing, 0.201 nm and 0.277 nm were identified by analyzing the inter-planar distance in the fringes seen in **Figure V-16d**.

Table V - 5: BET surface area analysis of two different types of CFMs.

	BET Surface Area/ $m^2 g^{-1}$	Langmuir Surface Area/ $m^2 g^{-1}$	Total Pore Volume/ $cm^3 g^{-1}$	Adsorption average pore width/ nm
CFM-1	525.98	829.18	0.324	2.46
CFM-2	684.25	1083.07	0.422	2.47

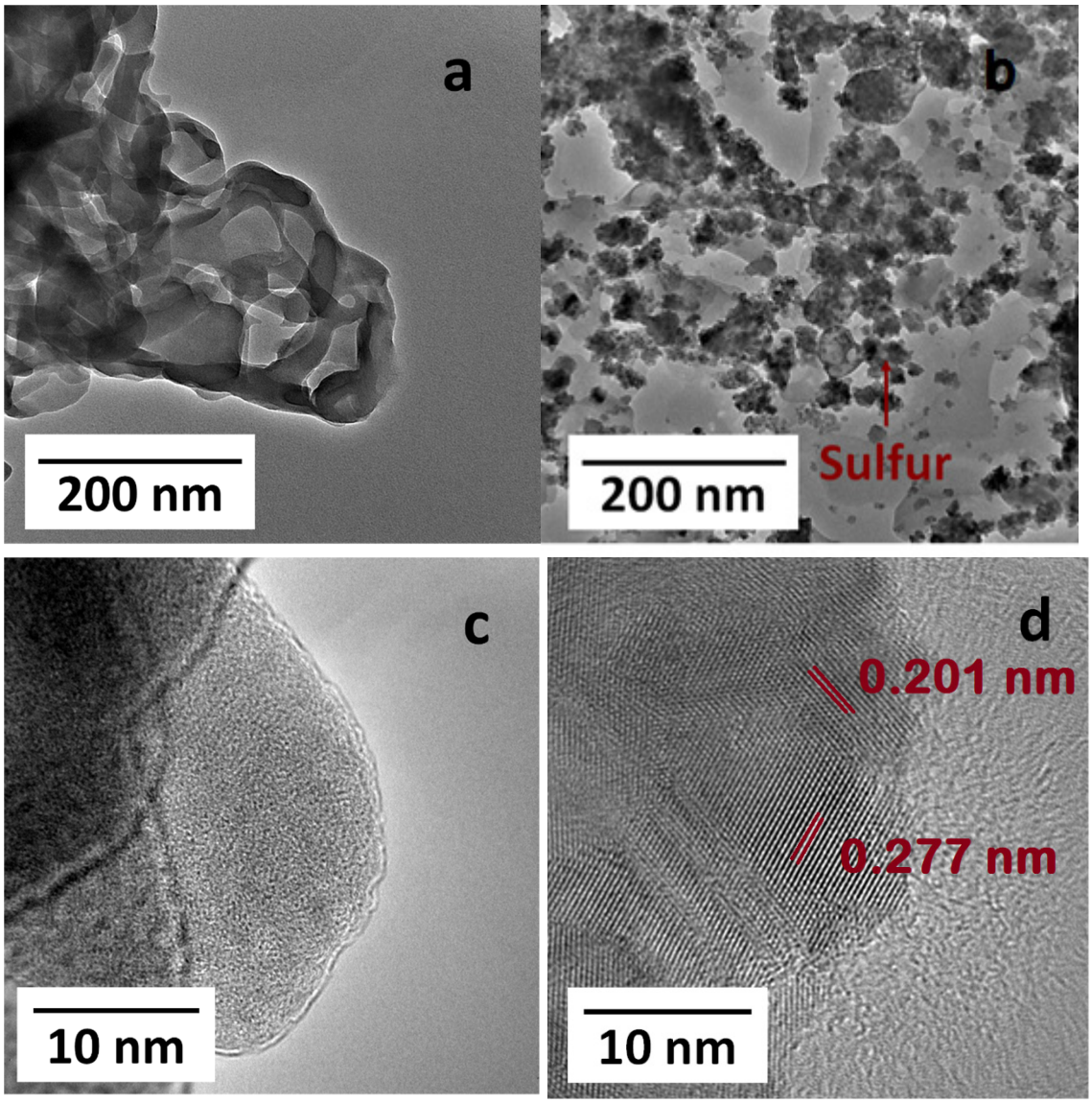

Figure V - 16: TEM images of CFM-1 and S –CFM-1 at different magnifications. (16a, 16c) CFM-1; (16b and 16d) S-CFM-1.

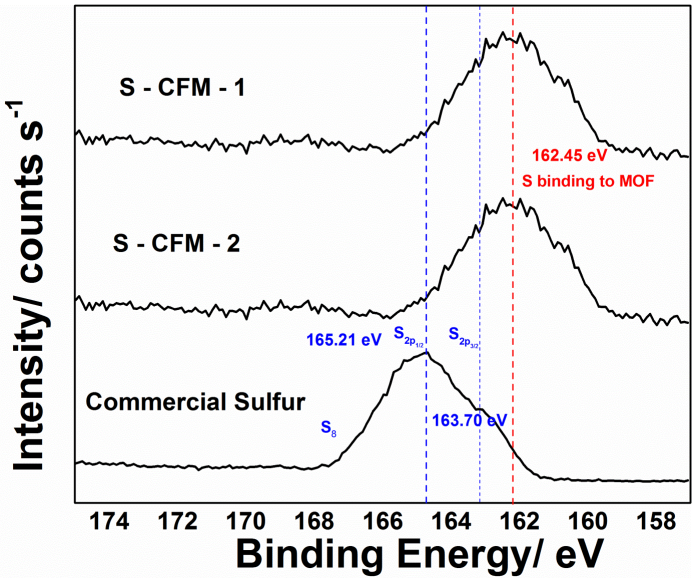

Figure V - 17: XPS S2p Binding Energy profile of Commercial Sulfur, S – CFM-1 and S – CFM-2.

The nature of sulfur in the S – CFMs was studied using XPS analysis (**Figure V-17**). XPS analysis was performed on a Thermo ESCALAB 250Xi with suitable background correction. It can be observed that the characteristic $S2p_{3/2}$ peak is observed for the commercial sulfur powder at 165.21 eV in line with previous reports for orthorhombic sulfur (S_8) [9-12]. The XPS spectra of S-CFMs show a shift in the S2p peak as compared to commercial sulfur indicating the absence of free elemental sulfur suggesting binding of sulfur to the CFM structures. The $S2p_{3/2}$ peak position at 162.45 eV corresponding to the binding of sulfur onto the CFMs is similar to values observed in chemically-bound sulfur studied by Chehimi et al.,[13] further confirming the bound nature of sulfur onto the CFMs. This chemical binding of sulfur along with the nanoporous nature of the CFMs is expected to result in minimal sulfur dissolution into the organic liquid electrolyte[14]. This effect has been observed in sulfur entrapped in single wall carbon nanotubes (SWCNTs) of ~1.5nm diameter by Fujimori et al [10] wherein sulfur adopts either a linear or a zig-zag orientation as opposed to the conventional cyclic S_8 rings of S. Due to an average pore size of 2 nm of CFMs, comparable to the SWCNTs (~2 nm) used, the sulfur strands might experience strain from the CFM pore walls thus yielding a lower S2p binding energy. The complete trapping of the polysulfide in a host matrix however, has not been reported in the literature and it is expected that further optimization of the CFM materials using a mechanistic understanding gained from the rest of this study would help engineer very high capacity cathodes with almost no capacity fade.

Though both CFM materials exhibit excellent cycling stability after initial stabilization, a significant portion of the initial observed capacity is lost within the 1st ten cycles. This loss in commercial sulfur is typically attributed to the dissolution of sulfur into the electrolyte and loss of the eventual polysulfide species. However, the stabilization of the capacity following the initial loss appears to draw credence to the possibility of the confinement occurring but the alluding to the possible existence or evidence of other extraneous sacrificial reactions. This result thus implied that the origin of the initial capacity loss in these S – CFMs needs to be better understood warranting better characterization to be conducted to be able to improve the overall performance of the CFM based sulfur electrode system.

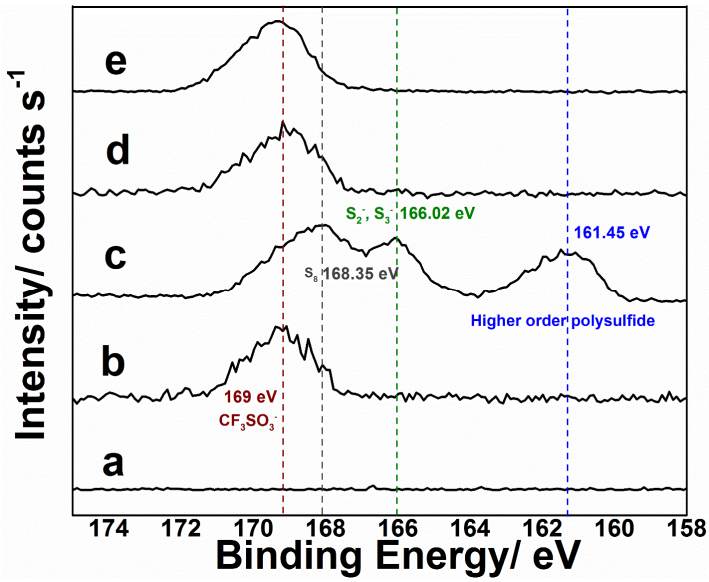

Figure V –18: XPS S2p binding energy profile of a) commercial separator b) commercial separator soaked in electrolyte; separators of c) commercial sulfur electrode; d) S – CFM-1; e) S – CFM-2 electrodes; (after 200 cycles at 0.2 C rate).

The effect of sulfur encapsulation within the CFM structures on the cycling performance of S – CFMs was therefore studied by analyzing the separators retrieved using XPS after 200 charge – discharge cycles. S2p peaks were analyzed to understand the nature of the sulfur/polysulfide species present in the various separators. As control experiments, the commercial separator and commercial separator dipped in the lithium electrolyte were also analyzed and the resultant XPS plots are shown in **Figure V-18 a,b**. As expected, the Celgard separator does not display an S2p peak before cycling while a distinct peak corresponding to the electrolyte species (Trifluoro methyl sulfonate lithium salt) is seen in **Figure V-18b**[15]. The XPS plot for the post-cycled separator for the commercial sulfur electrode shows S2p peaks at 168.35 eV, 166.02 eV and 161.45 eV. The peak at 168.35 eV corresponds to S2p peak of cyclic S_7, S_8. On the other hand, the peaks at 166.02 eV and 161.45 eV are due to lower and higher order polysulfide, respectively[16-19]. This indicates and validates the well-known phenomenon of the commercial sulfur electrode **(Figure V-18c)** undergoing rapid loss in capacity due to the rapid dissolution of polysulfide species formed because a lack of any medium or mechanism to retain/constrict the same at the electrode surface. However, the separators corresponding to the S – CFM electrodes (post-cycling, after 200 cycles) (**Figure V-18 (d, e)**) distinctly display only a single S2p peak at 169 eV which is attributed to the sulfur corresponding to the $LiCF_3SO_3$ from the electrolyte[15] as observed in the case of **Figure V-18b** for the commercial separator soaked in the electrolyte. The absence of any detectable polysulfide in the post-cycled separators cycled from electrodes generated with the CFM-1 and CFM-2, especially after 200 cycles (**Figure V-18 (d, e)**) indicates complete constriction of the formed polysulfide within the CFM structures possibly due to chemical-binding of S to the CFM architecture as observed in the TEM images (**Figure V-16**) and XPS (**Figure V-17**). In addition, spatial confinement (**Table V – 5**) possibly aids in ensuring polysulfide retention at the electrode. Though the porous structures have previously been shown to result in improved cycling behavior, complete masking of polysulfide dissolution using a porous host has seldom or never been reported to the best of our knowledge. The unique cage-like structure of the CFMs along with the chemical binding occurring therein thus results in a very stable cycling performance with a remarkably low fade rate of ~0.0014% $cycle^{-1}$.

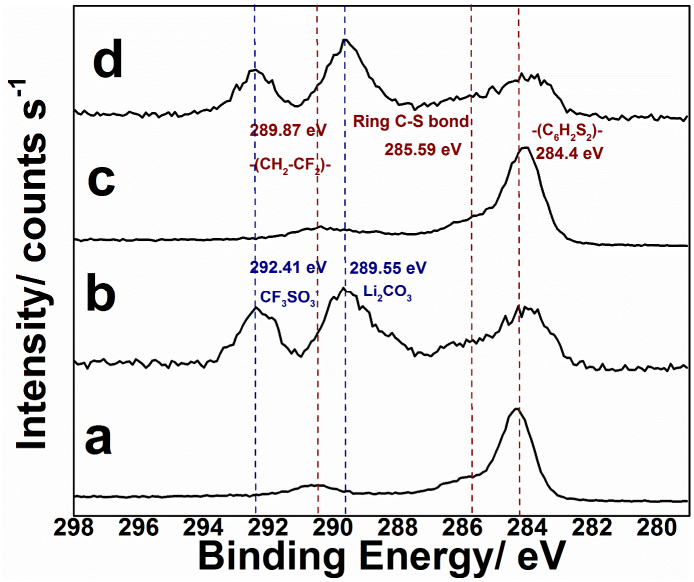

Figure V - 19: XPS C1s Binding Energy profile of slurry coated electrodes of a) S – CFM-1 before cycling, b) S –CFM-1 after 200 cycles, c) S – CFM-2 before cycling, and d) S – CFM-2 after 200 cycles at 0.2 C rate.

However, both the S-CFM electrodes generated with undergo initial loss in capacity which is typically known to occur and attributed to the polysulfide dissolution. The XPS results discussed above clearly indicate that this loss cannot be related to polysulfide dissolution as evidenced by the lack thereof of any sulfur species detected on the separators [**Figure V-19(d, e)**]. To understand the origin of this initial capacity loss observed, XPS was performed on both the S – CFM coated electrodes before and after 200 cycles. **Figure V-20** represents the C1s spectrum of slurry cast S – CFM electrodes and the same electrodes post cycling. S – CFM-1 (Figure V-20b) and S–CFM-2 (**Figure V-20d**) electrode samples have peaks corresponding to – (CF_2 – CF_2) – bonds from PVdF binder (289.87 eV)[20], -C_6H_5S- bond corresponding to ring C – S interactions (285.59 eV)[21] and –$C_6H_4S_2$- (284.4 eV)[22]. The presence of the C-S peaks herein confirms the observations in the S2p spectrum (Figure V-17) and corroborates the hypothesis that sulfur-carbon bonding aids in ensuring superior polysulfide retention within the CFM structure. The S – CFMs post-200 cycles showed two C_{1s} peaks at 292.41 eV and 289.55 eV in addition to the peaks observed before cycling. The peak at 292.41 eV corresponds to the $CF_3SO_3^-$group of the lithium salt $LiCF_3SO_3$ used with the organic electrolyte. The peak at 289.55 eV corresponds to Li_2CO_3 resulting from the irreversible reaction of Li^+ ions with the –(CO_3)- groups of the CFM.

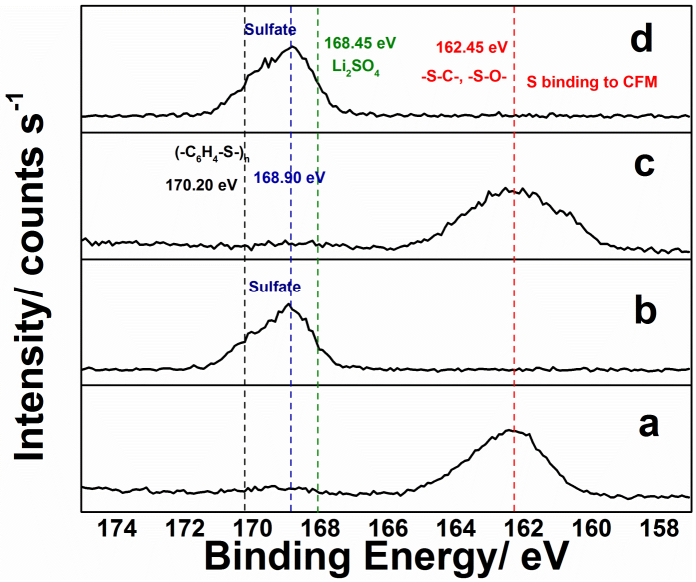

Figure V –20: XPS S2p Binding Energy profile of slurry coated electrodes of a) S – CFM-1-before cycling, b) S – CFM-1 after 200 cycles, c) S – CFM-2-before cycling and d) S – CFM-2 after 200 cycles at 0.2 C rate.

Figure V-20 depicts the S2p profiles of the S-CFM electrodes before and after cycling. Both S-CFM-1 and S-CFM-2 electrodes before cycling show S2p peak at 162.45 eV representing the bonding of sulfur to CFMs (as also observed in Figure V-17). Both S – CFM-1 and S –CFM-2 electrodes post-cycling however, show the presence of a satellite peak at 170.20 eV, corresponding to the occurrence of sulfur-carbon bonding [21, 24]. This indicates that sulfur is bound to the carbon before cycling as well as through the various stages of cycling preventing the loss of sulfur through polysulfide run-away to bulk electrolyte during cycling resulting in exceptional cycling stability. In addition to the peaks corresponding to C-S bonding, there are unique peaks observed in the post-cycled electrodes corresponding to the formation of a mixture of sulfate species. The irreversible loss in capacity could thus be attributed to irreversible consumption of sulfur through the formation of lithium, and other sulfates during electrochemical cycling. Thus, deactivation of the active material of sulfur occurs through the formation of sulfate species during the initial cycling resulting in irreversible capacity loss. The results presented herein clearly demonstrate that the embedding of sulfur into the nanoporous CFM frameworks directly in the as-prepared form without any carbonization step ensures minimal polysulfide transport out of the electrode into the separator ensuring minimal capacity loss because: (a) chemical bonding of carbon in the CFM structure with sulfur; and (b) constriction of the lithium polysulfide species within the porous matrix. This is indeed reflected resulting in stable capacity of ~609 mAh g^{-1} with a fade rate of only ~0.0014% cycle $^{-1}$ demonstrating the promise of this novel synthetic strategy. Based on the insight gained from this study sulfur infiltrated framework materials (SFM) with higher ionic conductivities were developed and upon testing showed an initial capacity of 1626 mAh/g with stable performance of 1044 mAh/g for over 100 cycles (**Figure V-21**). As an additional subtask of Phase-2, an air – stable inorganic framework material (IFM) was explored to trap polysulfides (Figure V-22a shows the XRD patterns of S doped IFM). The IFMs exhibit very high (80%) S infiltration and a low irreversible capacity loss of 15%. Further, the IFMs improved the first cycle specific capacity of S to ~1250 mAh/g stabilizing at ~750 mAh/g (**Figure V-22b**). The improved specific capacity of the sulfur electrode is attributed to the successful polysulfide trapping by IFMs and work is currently on-going to improve the performance further, the results of which will be reported in future reports.

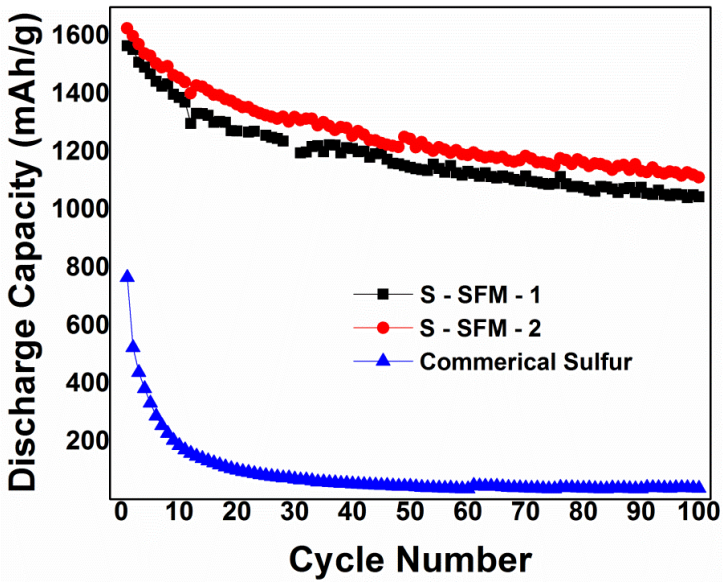

Figure V -21: Cycling performance of Sulfur – infiltrated framework material (SFM).

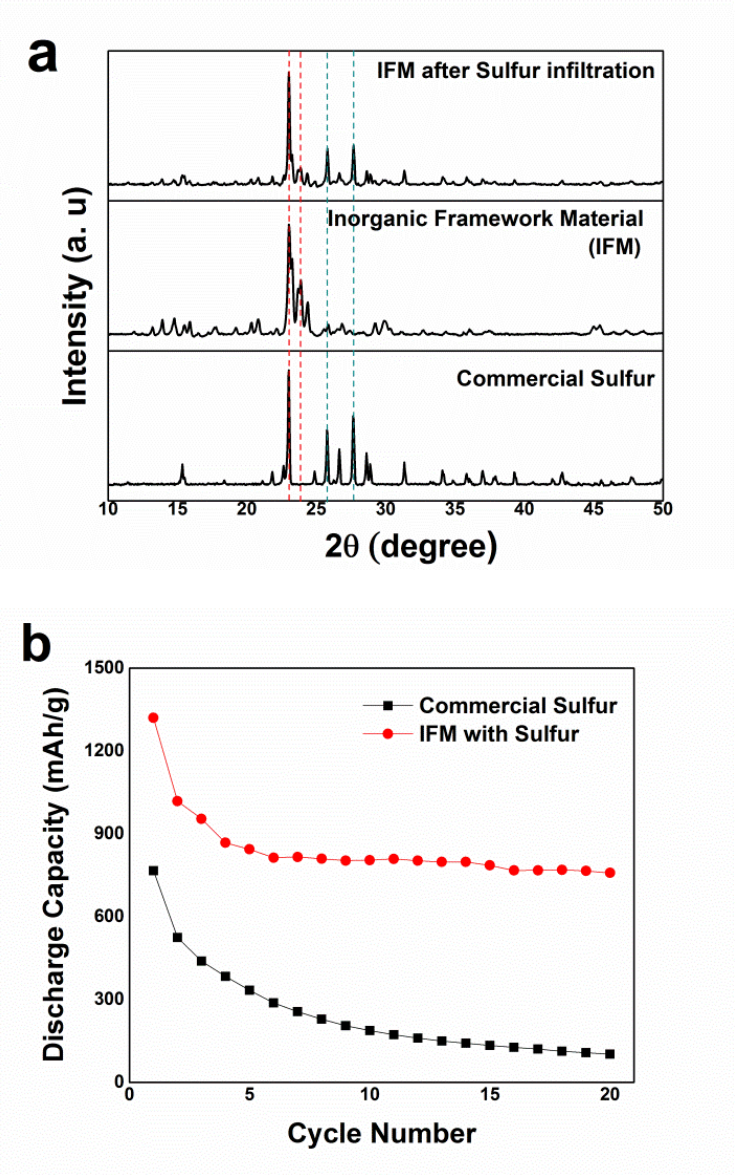

Figure V -22: (a) XRD patterns showing the infiltration of Sulfur into the Inorganic Framework Material (IFM) showing retention of IFM structure. (b) Cycling behavior of Sulfur infiltrated IFM.

FY 2017 – (Q1-Q4)

Phase-3 involved comprehensive study of the physical and chemical properties of the Composite Polymer Electrolytes (CPEs) developed in Phase-2 with three nano fillers. The CPEs when tested against commercial sulfur cathodes demonstrated very stable capacity of ~812 mAh/g after 100 cycles with minimal fade rate of 0.012%/cycle. The mechanical property analysis showed that the CPEs showed 2-3 times improvement in tensile strength as compared to their counterparts synthesized using conventional technique (**Figure V- 23**).

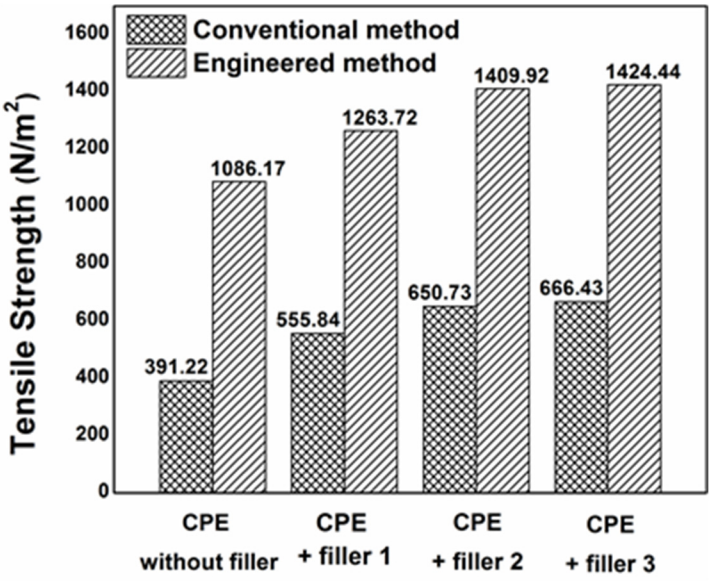

Figure V-23. Cycling performance of Sulfur – infiltrated framework material (SFM)

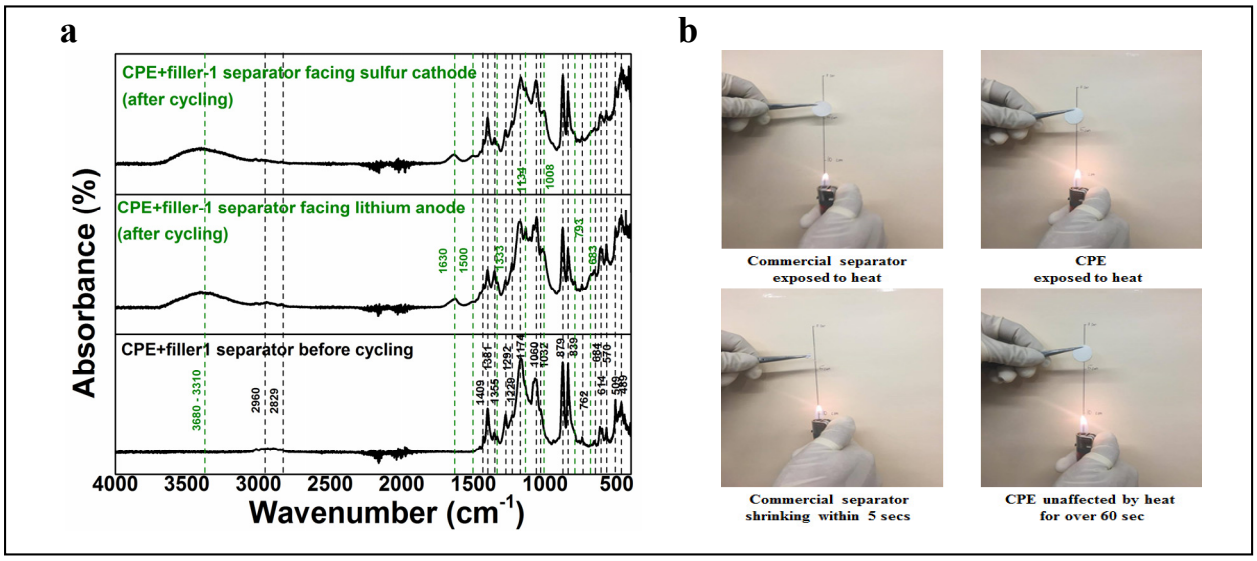

Figure V-24a. FT-IR spectra of CPE after cycling and Figure 2b flammability test result of the CPE.

The CPEs also showed excellent chemical stability with minimal modification to the polymer backbone after cycling confirmed by FT-IR spectroscopy (FT-IR) (**Figure V-24a**) and good flammability properties as compared to commercial battery separator (**Figure V-24b**).

In addition, Phase-3 also involved development of Directly Doped Sulfur Architecture (DDSA) electrode with very high sulfur loadings of ~18 mg/cm^2 and generation of Polysulfide Trapping Agent (PTA) coated DDSA electrodes with excellent polysulfide trapping property depicted in **Figure V-25**.

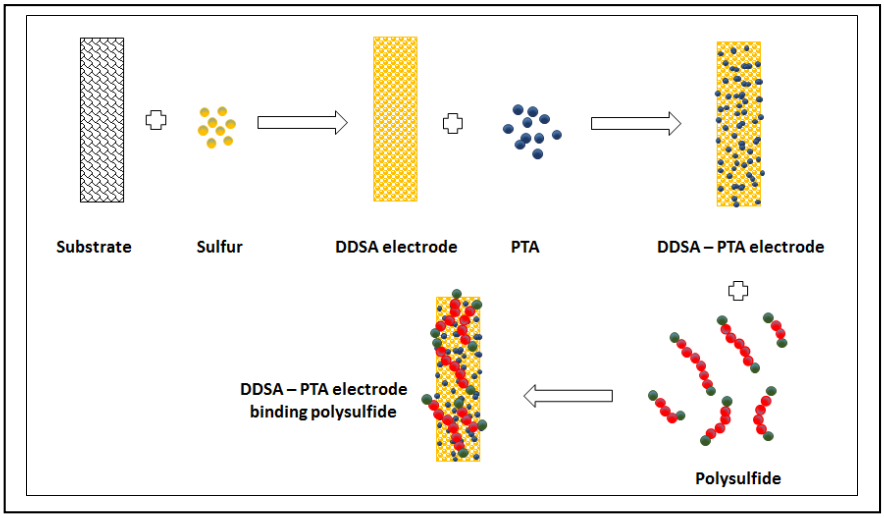

Figure 25. Scheme of interaction of PTA with polysulfide.

The PTA coated DDSA electrode shows excellent electrochemical cycling performance with an initial capacity of 1305 mAh/g that stabilized at 1112 mAh/g to 200 cycles with less than 0.0014% when cycled at 0.2C rate (**Figure V-26**). The initial fade of ~0.2% likely due to parasitic reactions will be overcome by further optimization.

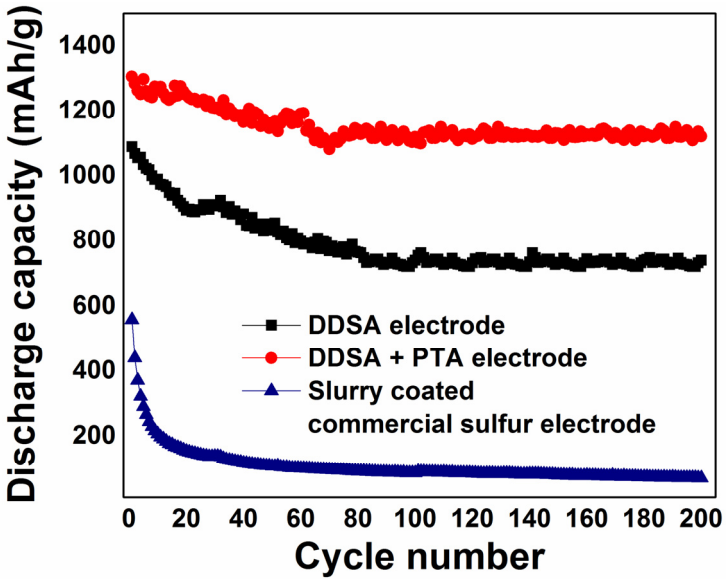

Figure V-26. Cycling performance of PTA coated DDSA electrode

The UV-VIS spectrum of PTA-DDSA (**Figure V-27a**) showed considerable decrease in the intensities of peaks corresponding to the higher and lower order polysulfides as opposed to the slurry coated electrode suggesting effective adsorption of the polysulfide by the PTA via physical/chemical binding. XPS study of the electrodes after 200 electrochemical charge – discharge cycles (**Figure V-27b**) clearly shows the absence of polysulfide peaks showing the efficacy of the polysulfide trapping agents in completing eliminating polysulfide dissolution.

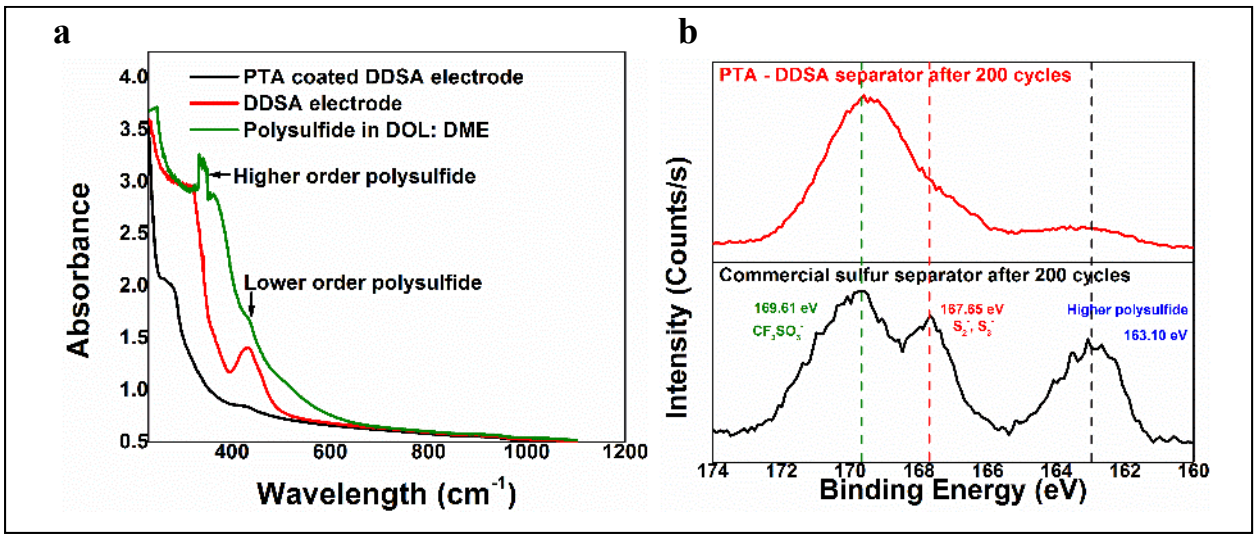

Figure V-27a: UV – VIS spectroscopy of PTA coated DDSA electrodes showing absence of polysulfide absorbance and Figure 5b: Comparison of XPS patterns of commercial sulfur and PTA - DDSA separators after 200 cycles.

A new sulfonic Complex Framework Material (CFM) was also designed, synthesized and characterized for electrochemical response. **Figure V-28a** shows the XRD pattern of the CFM compared with the pattern simulated using the crystallographic information file (CIF). The CFMs demonstrated a high sulfur loading of ~ 3-4 mg/cm^2 and maintained a capacity of 1051 mAh/g for over 100 cyces with 0.0011% fade at 0.2C rate (**Figure V-28b**).

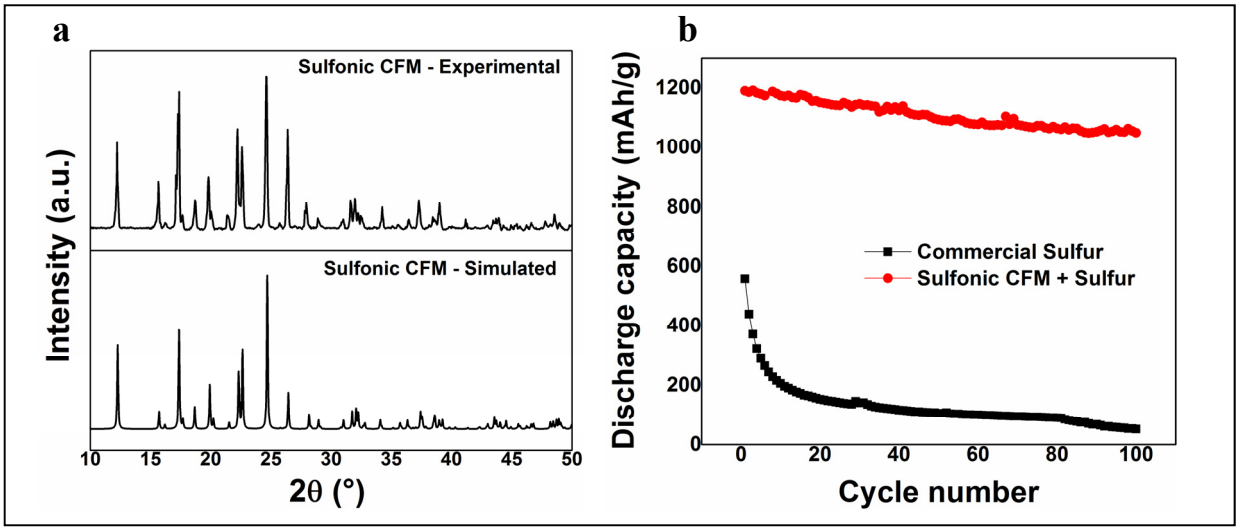

Figure V-28a. Comparison of experimental and simulated XRD patterns of sulfonic CMS Figure 6b Electrochemical cycling performance of the sulfonic CFM compared with commercial sulfur.

Manufacturing cost analysis of the various electrode materials (sulfur hosted composite framework materials (CFM), PTA coated DDSA and the LIC coated sulfur nanoparticles), separators (nanofiller incorporated CPE,

CFM added gel polymer electrolyte (GPE) and all solid LIC) and electrolytes developed during Phase 1-3 of the project was accordingly conducted to assess the scalabilty of all the laboratory derived materials. Prismatic pouch cells (4 mAh full cell) are currently being assembled and tested using the Phase-3 optimized systems. Accordingly, the PTA-DDSA materials as discussed above demonstrate the best electrochemical performance exhibiting stable capacity ~1112 mAh/g after 200 cycles with less than 0.0014% when cycled at 0.2C rate. This system will therefore, be selected for testing in pouch cells.

Conclusions

The aim of Phase-1 was to establish methods to improve sulfur cycling characteristics by use of lamination approaches, especially in the form of LIC materials. It can clearly be observed that fade rates have been significnalty reduced by using the 4 approaches in Phase-1 described above. Stable capacities of in excess of 600 mAh/g have been observed in two systems with stability for over 150 cycles, the flexible sulfur-polymer composite electrodes and the Sulfur CFM materials. Exceptionally low fade rates of ~0.003%/cycle have been observed which greatly supports the hypothesis of LIC-based engineering.

The aim of Phase-2 was to establish methods to improve sulfur cycling characteristics by employing interface engineering strategies and use of framework structures. In addition, the work was directed at developing doped LIC materials and doped sulfur nanoparticles. By implementing such approaches various materials have been derived with initial capacities in excess of 1400 mAh/g with retention of >1000 mAh/g after 100 cycles. It can also be clearly observed that fade rates have been significantly reduced by using the four approaches in Phase-2 described above. Exceptionally low fade rates of ~0.0014% loss per cycle have been observed and in the case of CFM materials a complete absence of polysulfides at the separator has been shown after 200 cycles.

The aim of Phase-3 was to establish methods to improve sulfur cycling characteristics by replacing the commercial separator and electrolyte using a novel composite polymer electrolyte containing nanoscale fillers serving to provide improved mechanical strength, Li-ion conductivity and flame resistances. In addition, the work was directed at developing doped sulfur architectures with improved electronic conductivity, and complex framework materials as effective polysulfide trapping agents. By implementing such simple and scalable approaches, various materials have been generated with initial capacities close to 1400 mAh/g with retention of capacity >1100 mAh/g after 200 cycles. It can also be clearly observed that fade rates have been significantly reduced by using these novel approaches and exceptionally low fade rates of ~0.0014% loss per cycle have been obtained. Furthermore, in the case of PTA coated DDSA systems, a complete absence of polysulfides at the separator has been shown after 200 cycles demonstrating the promise of this system for use in full cell fabrication against an engineered dendrite free lithium metal anode. Such a combined system will likely exhibit performance characteristics of ~400 Wh/kg meeting the Batt 500 goals.

Key Publications

1. P. J. Hanumantha, B. Gattu, et al., Journal of The Electrochemical Society, 2014, 161, A1173-A1180.
2. Jampani, P.H.; Gattu, B.; Shanthi, P.M.; Kumta, P.N. Novel electro-spun sulfur wires for fabricating mattes of lithium-sulfur batteries, International Patent Number: WO 2016/145429 A1 (Awarded: September 15, 2016).
3. Jampani, P.H.; Shanthi, P.M.; Gattu, B.; Kumta, P.N. Novel Flexible Sulfur Wire Fabrics (FSF) for Lithium-Sulfur Batteries, The Electrochemical Society (Spring 2015), Chicago, IL.
4. Shanthi, P.M.; Jampani, P.H.; Gattu, B.; Velikokhatnyi, O.I.; Kumta, P.N. Effect of Coating and Particle Properties on the Cycling Stability of Li-Ion Conductor (LIC) Coated Sulfur Cathodes, The Electrochemical Society (Spring 2015), Chicago, IL.
5. Shanthi, P.M.; Jampani, P.H.; Gattu, B.; Velikokhatnyi, O.I.; Kumta, P.N. Doped Lithium Orthosilicates - Promising High Rate Lithium-Ion Conductors for Li-S Batteries, The Electrochemical Society (Fall 2016), Honolulu, HI

6. Shanthi, P.M; Jampani, P.H; Gattu, B; Sweeney, M; Datta, M.K; Kumta, P.N. Nanoporous Non-Carbonized Metal Organic Frameworks (MOFs): Effective Sulfur Hosts for High Performance Li-S Batteries, manuscript submitted (2016).
7. Jampani, P.H.; Gattu, B.; Shanthi, P.M.; Damle, S.S.; Basson, Z.; Bandi, R.; Datta, M.K.; Park, S.K.; Kumta, P.N. Flexible sulfur wires (Flex-SWs) – A Versatile platform for lithium-sulfur batteries, Electrochimica Acta Vol. 212, pp. 286 - 293 (2016)
8. Shanthi, P.M; Jampani, P.H; Gattu, B; Sweeney, M; Datta, M.K; Kumta, P.N. Nanoporous Non-Carbonized Metal Organic Frameworks (MOFs): Understanding the Origin of Irreversible Capacity loss in Non-Carbonized Carbonate − based Metal Organic Framework (MOF) Sulfur hosts for Lithium − Sulfur battery, Electrochimica Acta, Vol, 229, pp 208–218 (2017)
9. Shanthi, P. M, Jampani, P.H., Gattu, B.; Datta, M K, Velikokhatnyi, O. I., Kumta, P.N., "Electrospinning of PVdF-HFP: Novel Composite Polymer Electrolytes (CPEs) with enhanced ionic conductivities for Lithium-Sulfur batteries." U.S. Provisional Appln. Serial No. 62/529,638 (2017).
10. Jampani, P.H., Shanthi, P. M., Gattu, B., Datta, M K, Velikokhatnyi, O.I., Kumta, P.N., "High capacity, air-stable, Structurally Isomorphous lithium Alloy (SIA), Multilayer Porous Foams (MPFs) and Composite Multilayer Anodes (CMAs) for dendrite-free lithium metal anodes for Li-ion batteries", U.S. Provisional Patent Appln. No. 62/529,588 (2017).
11. Shanthi, P.M., Jampani, P.H., Gattu, B., Albuquerque T., Datta, M.K., Kumta, P.N., "Novel electrospun PVdF – HFP Composite Polymer Electrolytes (CPEs) with enhanced Ionic Conductivities for Lithium – Sulfur batteries", ACS Applied Energy Materials, 2017
12. Shanthi, P.M., Jampani, P.H., Gattu, B., Datta, M.K., Velikokhatnyi, O.I., Kumta, P.N., "The effect of Mg, Ca and F doping on the ionic conductivity of Li4SiO4: Experimental and First Principles Investigation", Solid State Ionics (2017) under review.

References

1. Ji, X.; Nazar, L. F., Advances in Li-S batteries. Journal of Materials Chemistry 2010, 20 (44), 9821-9826.

2. Miao, L.-X.; Wang, W.-K.; Wang, A.-B.; Yuan, K.-G.; Yang, Y.-S., A high sulfur content composite with core-shell structure as cathode material for Li-S batteries. Journal of Materials Chemistry A 2013, 1 (38), 11659-11664.

3. Wang, H.; Yang, Y.; Liang, Y.; Robinson, J. T.; Li, Y.; Jackson, A.; Cui, Y.; Dai, H., Graphene-Wrapped Sulfur Particles as a Rechargeable Lithium–Sulfur Battery Cathode Material with High Capacity and Cycling Stability. Nano Letters 2011, 11 (7), 2644-2647.

4. Wang, Z.; Dong, Y.; Li, H.; Zhao, Z.; Bin Wu, H.; Hao, C.; Liu, S.; Qiu, J.; Lou, X. W., Enhancing lithium–sulphur battery performance by strongly binding the discharge products on amino-functionalized reduced graphene oxide. Nat Commun 2014, 5.

5. Chen, R.; Zhao, T.; Tian, T.; Cao, S.; Coxon, P. R.; Xi, K.; Fairen-Jimenez, D.; Vasant Kumar, R.; Cheetham, A. K., Graphene-wrapped sulfur/metal organic framework-derived microporous carbon composite for lithium sulfur batteries. APL Materials 2014, 2 (12), 124109.

6. Chen, S.-R.; Zhai, Y.-P.; Xu, G.-L.; Jiang, Y.-X.; Zhao, D.-Y.; Li, J.-T.; Huang, L.; Sun, S.-G., Ordered mesoporous carbon/sulfur nanocomposite of high performances as cathode for lithium–sulfur battery. Electrochimica Acta 2011, 56 (26), 9549-9555.

7. Jayaprakash, N.; Shen, J.; Moganty, S. S.; Corona, A.; Archer, L. A., Porous Hollow Carbon@Sulfur Composites for High-Power Lithium–Sulfur Batteries. Angewandte Chemie 2011, 123 (26), 6026-6030.

8. Li, X.; Cao, Y.; Qi, W.; Saraf, L. V.; Xiao, J.; Nie, Z.; Mietek, J.; Zhang, J.-G.; Schwenzer, B.; Liu, J., Optimization of mesoporous carbon structures for lithium-sulfur battery applications. Journal of Materials Chemistry 2011, 21 (41), 16603-16610.

9. Yu, X.-R.; Liu, F.; Wang, Z.-Y.; Chen, Y., Auger parameters for sulfur-containing compounds using a mixed aluminum-silver excitation source. Journal of Electron Spectroscopy and Related Phenomena 1990, 50 (2), 159-166.

10. Fujimori, T.; Morelos-Gómez, A.; Zhu, Z.; Muramatsu, H.; Futamura, R.; Urita, K.; Terrones, M.; Hayashi, T.; Endo, M.; Young Hong, S.; Chul Choi, Y.; Tománek, D.; Kaneko, K., Conducting linear chains of sulphur inside carbon nanotubes. Nat Commun 2013, 4.

11. Hollinger, G.; Kumurdjian, P.; Mackowski, J. M.; Pertosa, P.; Porte, L.; Duc, T. M., ESCA study of molecular GeS3-x Tex As2 glasses. Journal of Electron Spectroscopy and Related Phenomena 1974, 5 (1), 237-245.

12. Thomas, J. M.; Adams, I.; Williams, R. H.; Barber, M., Valence band structures and core-electron energy levels in the monochalcogenides of gallium. Photoelectron spectroscopic study. Journal of the Chemical Society, Faraday Transactions 2: Molecular and Chemical Physics 1972, 68 (0), 755-764.

13. Chehimi, M. M.; Delamar, M., X-ray photoelectron spectroscopy of merocyanine dyes. Journal of Electron Spectroscopy and Related Phenomena 1990, 50 (2), C25-C32.

14. Yang, C.-P.; Yin, Y.-X.; Guo, Y.-G.; Wan, L.-J., Electrochemical (De)Lithiation of 1D Sulfur Chains in Li–S Batteries: A Model System Study. Journal of the American Chemical Society 2015, 137 (6), 2215-2218.

15. Lindberg, B. J.; Hamrin, K.; Johansson, G.; Gelius, U.; Fahlman, A.; Nordling, C.; Siegbahn, K., Molecular Spectroscopy by Means of ESCA II. Sulfur compounds. Correlation of electron binding energy with structure. Physica Scripta 1970, 1 (5-6), 286.

16. Liang, X.; Hart, C.; Pang, Q.; Garsuch, A.; Weiss, T.; Nazar, L. F., A highly efficient polysulfide mediator for lithium–sulfur batteries. Nat Commun 2015, 6.

17. Zu, C.; Fu, Y.; Manthiram, A., Highly reversible Li/dissolved polysulfide batteries with binder-free carbon nanofiber electrodes. Journal of Materials Chemistry A 2013, 1 (35), 10362-10367.

18. Su, Y.-S.; Fu, Y.; Cochell, T.; Manthiram, A., A strategic approach to recharging lithium-sulphur batteries for long cycle life. Nat Commun 2013, 4.

19. Zu, C.; Azimi, N.; Zhang, Z.; Manthiram, A., Insight into lithium-metal anodes in lithium-sulfur batteries with a fluorinated ether electrolyte. Journal of Materials Chemistry A 2015, 3 (28), 14864-14870.

20. Dapoz, S.; Betz, N.; Guittet, M.-J.; Le Moël, A., ESCA characterization of heparin-like fluoropolymers obtained by functionalization after grafting induced by swift heavy ion irradiation. Nuclear Instruments and Methods in Physics Research Section B: Beam Interactions with Materials and Atoms 1995, 105 (1–4), 120-125.

21. Riga, J.; Snauwaert, P.; De Pryck, A.; Lazzaroni, R.; Boutique, J. P.; Verbist, J. J.; Brédas, J. L.; André, J. M.; Taliani, C., Electronic structure of sulphur-containing conducting polymers. Synthetic Metals 1987, 21 (1–3), 223-228.

22. Huntley, D. R., The mechanism of the desulfurization of benzenethiol by nickel (110). The Journal of Physical Chemistry 1992, 96 (11), 4550-4558.

23. Cavanagh, A. S.; Lee, Y.; Yoon, B.; George, S., Atomic Layer Deposition of LiOH and Li2CO3 Using Lithium t-Butoxide as the Lithium Source. ECS Transactions 2010, 33 (2), 223-229.

24. Gardella, J. A.; Ferguson, S. A.; Chin, R. L., $\pi^* \leftarrow \pi$ Shakeup Satellites for the Analysis of Structure and Bonding in Aromatic Polymers by X-Ray Photoelectron Spectroscopy. Appl. Spectrosc. 1986, 40 (2), 224-232.